Supplementary Information

Pt/IrO_x enables selective electrochemical C-H chlorination at high current

Bo Wu[1,2,7], Ruihu Lu[3,7], Chao Wu[4,7], Tenghui Yuan[5], Bin Liu[6], Xi Wang[1], Chenyi Fang[1], Ziyu Mi[4], Surani Bin Dolmanan[2], Weng Weei Tjiu[2], Mingsheng Zhang[2], Bingqing Wang[1], Zainul Aabdin[2], Sui Zhang[1], Yi Hou[1], Bote Zhao[5], Shibo Xi[4], Wan Ru Leow[4*], Ziyun Wang[3*] and Yanwei Lum[1,2*]

[1]Department of Chemical and Biomolecular Engineering, National University of Singapore, Singapore, 117580, Republic of Singapore.

[2]Institute of Materials Research and Engineering (IMRE), Agency for Science, Technology and Research (A*STAR), 2 Fusionopolis Way, Innovis #08-03, Singapore 138634, Republic of Singapore.

[3]School of Chemical Sciences, The University of Auckland, Auckland, 1142, New Zealand.

[4]Institute of Sustainability for Chemical, Energy and Environment, Agency for Science, Technology and Research (A*STAR), 1 Pesek Road, 627833, Republic of Singapore.

[5]School of Environment and Energy, South China University of Technology, Guangzhou, 510006, China.

[6]Department of Chemical and Environmental Engineering, Yale University, 06520, 810 West Campus Drive, West Haven, CT 06516, United States.

[7]These authors contributed equally to this work.

*Corresponding author: wanru_leow@isce2.a-star.edu.sg

*Corresponding author: ziyun.wang@auckland.ac.nz

*Corresponding author: lumyw@nus.edu.sg

Supplementary Note 1

Local pH calculations

Since KCl is a non-buffering electrolyte, the local pH at the electrode surface likely differs significantly from the bulk when a current is applied. Therefore, we performed local pH calculations, implemented using Matlab R2023a[42]. The results show that the local pH does indeed become more acidic with a higher current density. During the reaction, H^+ is generated by the anode and the relevant reaction equations are listed below:

$$Cl^- - 2e^- + R-H \leftrightarrow R-Cl + H^+$$

$$Cl^- - 2e^- + H_2O \leftrightarrow ClO^- + 2H^+$$

$$2H_2O - 4e^- \leftrightarrow O_2 + 4H^+$$

We use film theory for the electrolyte-electrode boundary layer, in which velocity gradients or convective effects are assumed to be negligible. Thus, the equation can be set as follows:

$$H^+_{formation} = \left(\frac{cef_{R-Cl}}{zef_{R-Cl}} + 2\left(\frac{cef_{ClO^-}}{zef_{ClO^-}}\right) + 4\left(\frac{cef_{O_2}}{zef_{O_2}}\right)\right)$$

The boundary conditions of this equation in different electrolytes are briefly introduced below.

At time t > 0 and x = 0 (the interface of bulk solution and the boundary layer):

The electrolytes are 1.0 M KCl, which has no buffering ability, thus the concentration of H^+ for KCl is 10^{-7};

At time t > 0 and x = δ (the electrolyte surface)

The current density determines the generation rate of H^+ on the electrode surface. Thus, the boundary conditions of these equations are similar in the same halide ion electrolyte. Matlab

R2023a was used to calculate the concentration distribution of H^+ on the electrode surface, and the surface local pH was obtained. The local pH values of different current are shown in Fig. S47.

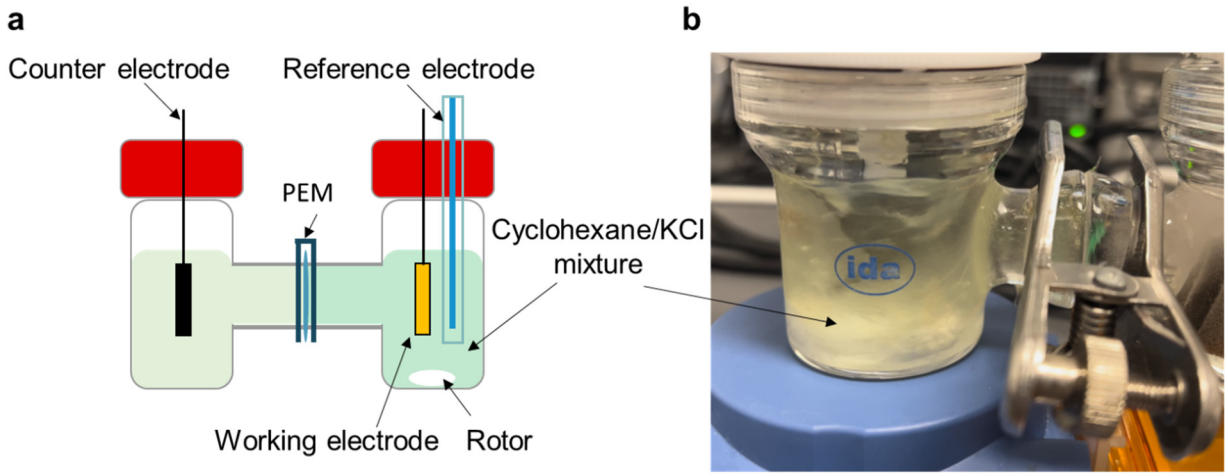

Fig. S1. (a) Schematic illustration of chlorocyclohexane production in the H-type cell. (b) Picture of H-type cell during the reaction. To ensure good mixing of the emulsion, a high rotation speed (500 rpm) was used to maintain rapid agitation.

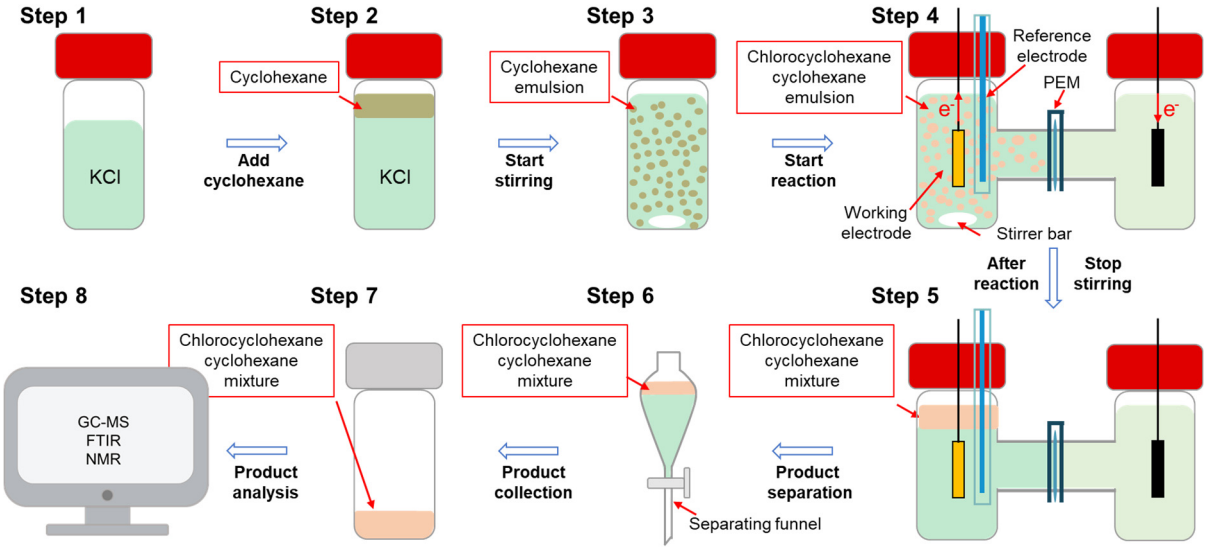

Fig. S2. Schematic illustration of the process for conversion of cyclohexane to chlorocyclohexane.

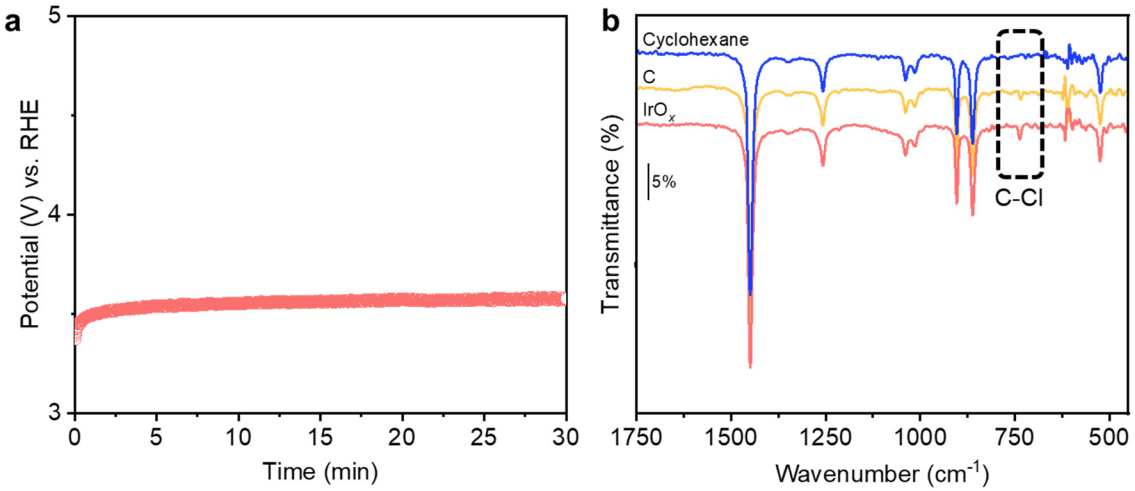

Fig. S3. (a) Applied potential to the C sheet anode as a function of time at a constant current of 300 mA. (b) FTIR spectroscopy of samples obtained using C and IrO_x. Note: The IrO_x is coated onto a Ti mesh.

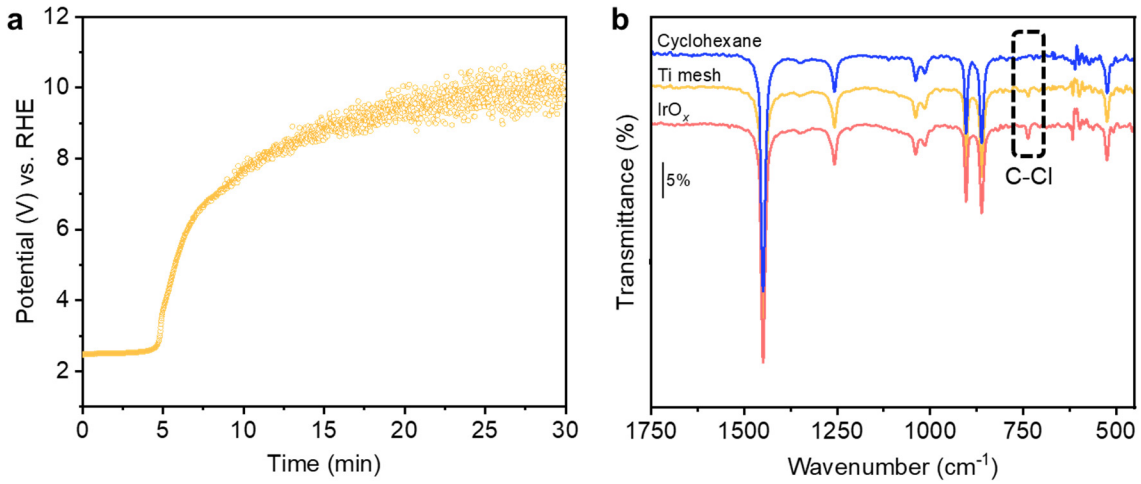

Fig. S4. (a) The potential applied to the Ti mesh as a function of time at a constant current of 300 mA. (b) FTIR spectroscopy of samples obtained using Ti and IrO_x.

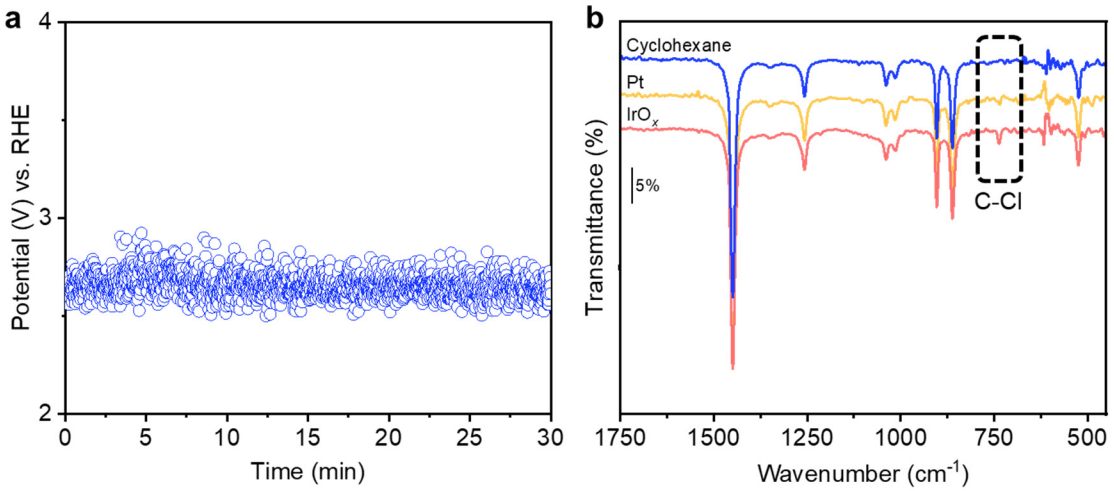

Fig. S5. (a) The potential applied to the Pt foil as a function of time at a constant current of 300 mA. (b) FTIR spectroscopy of samples obtained using Pt and IrO_x.

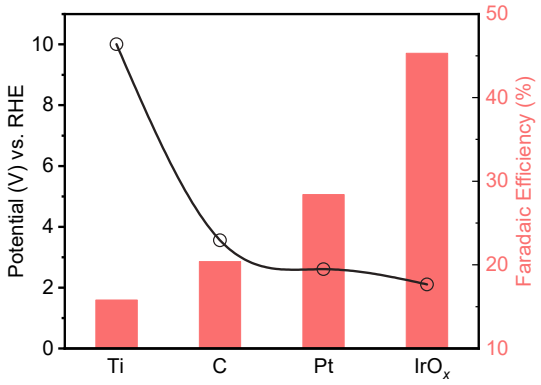

Fig. S6. Comparison of chlorocyclohexane production for the different anodes under a current of 300 mA.

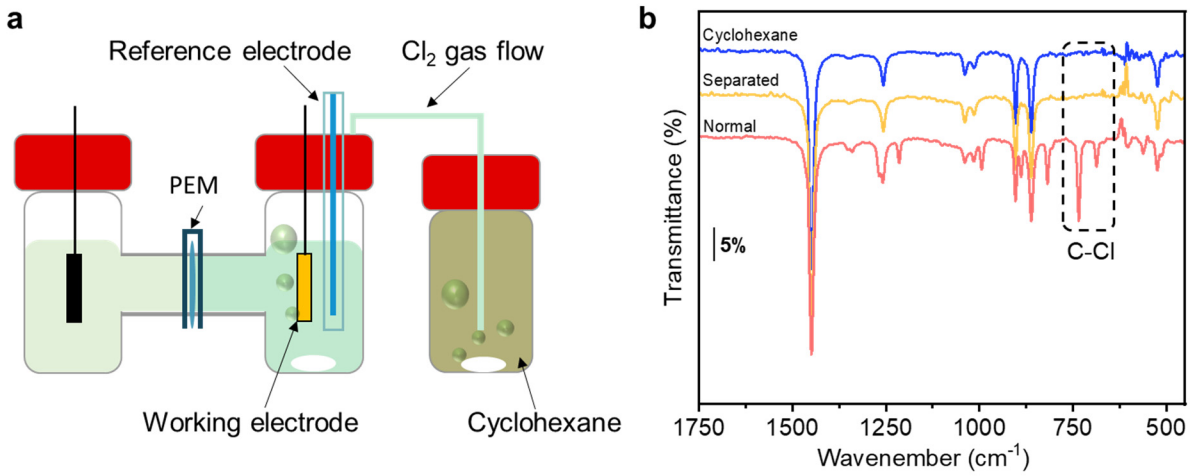

Fig. S7. (a) Schematic illustration of the control experiment where Cl_2 is generated via electrolysis and directly purged into a separate solution containing cyclohexane. This is termed as the 'Separated' condition. (b) Comparison of FTIR spectroscopy results obtained under the different conditions under 800 mA. 'Normal' represents the typical case in which the cyclohexane was added to KCl and used as the electrolyte.

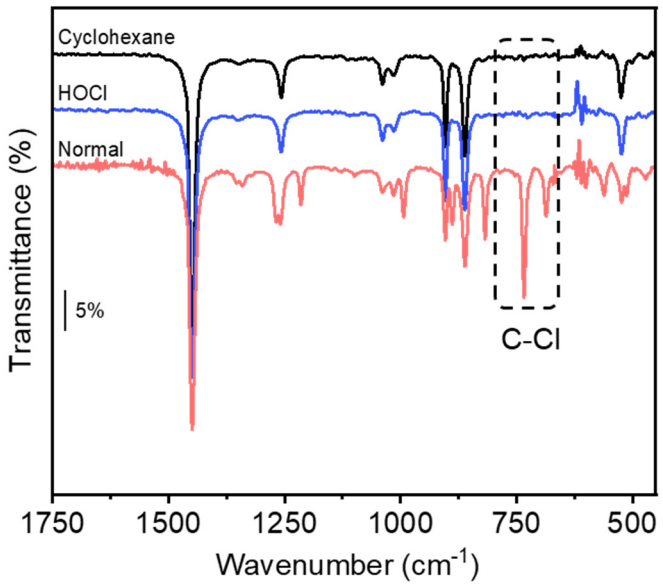

Fig. S8. Comparison of the FTIR spectroscopy results obtained under different conditions at 1000 mA. 'Normal' represents the typical case in which cyclohexane was added to 1 M KCl and used as the electrolyte. 'HOCl' represents the control case whereby Cl_2 evolution was first performed to generate a HOCl solution. Cyclohexane was subsequently added to this HOCl solution with stirring but without any applied current.

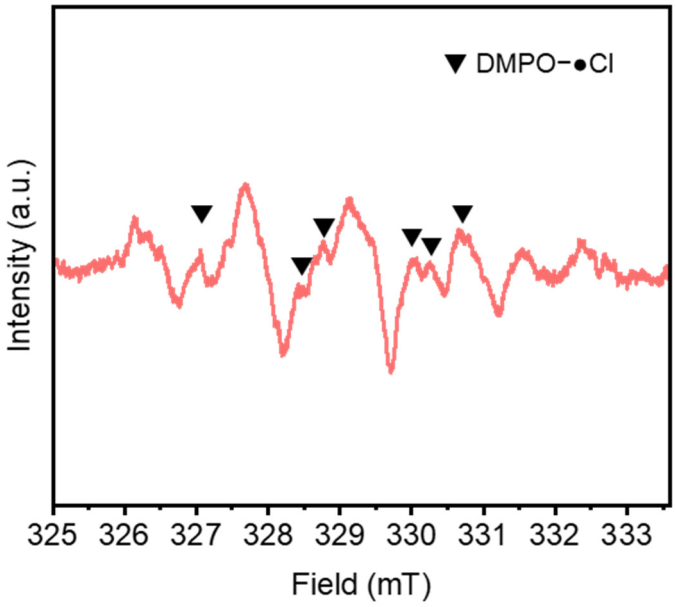

Fig. S9. EPR spectra of the electrolyte containing 0.1 mM of DMPO in 1 M KCl solution using IrO_x as the electrode with a duration of 4 min.

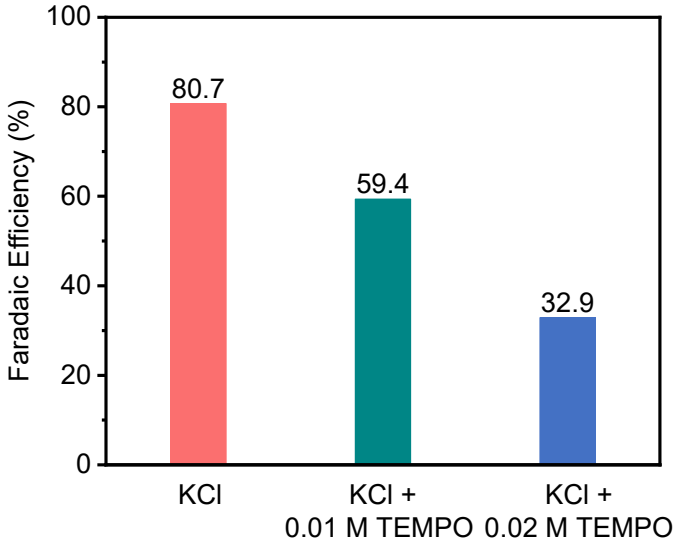

Fig. S10. Chlorocyclohexane FE obtained with electrolyte containing 0.01 M or 0.02 M of TEMPO at a current of 800 mA.

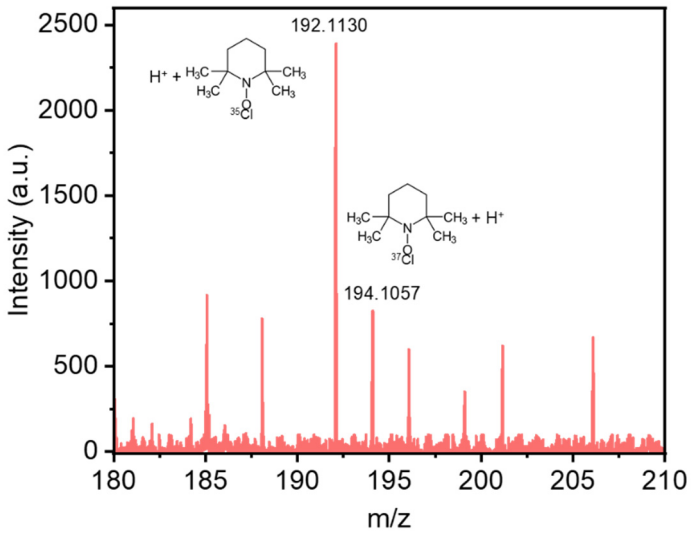

Fig. S11. Electrospray ionization–high-resolution mass spectrometry results of the sample using TEMPO as the radical trap.

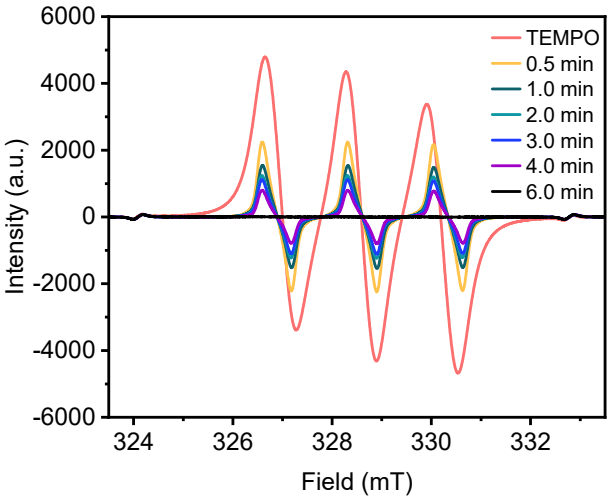

Fig. S12. EPR signals of the electrolyte for the C anode after different reaction times with a current of 400 mA.

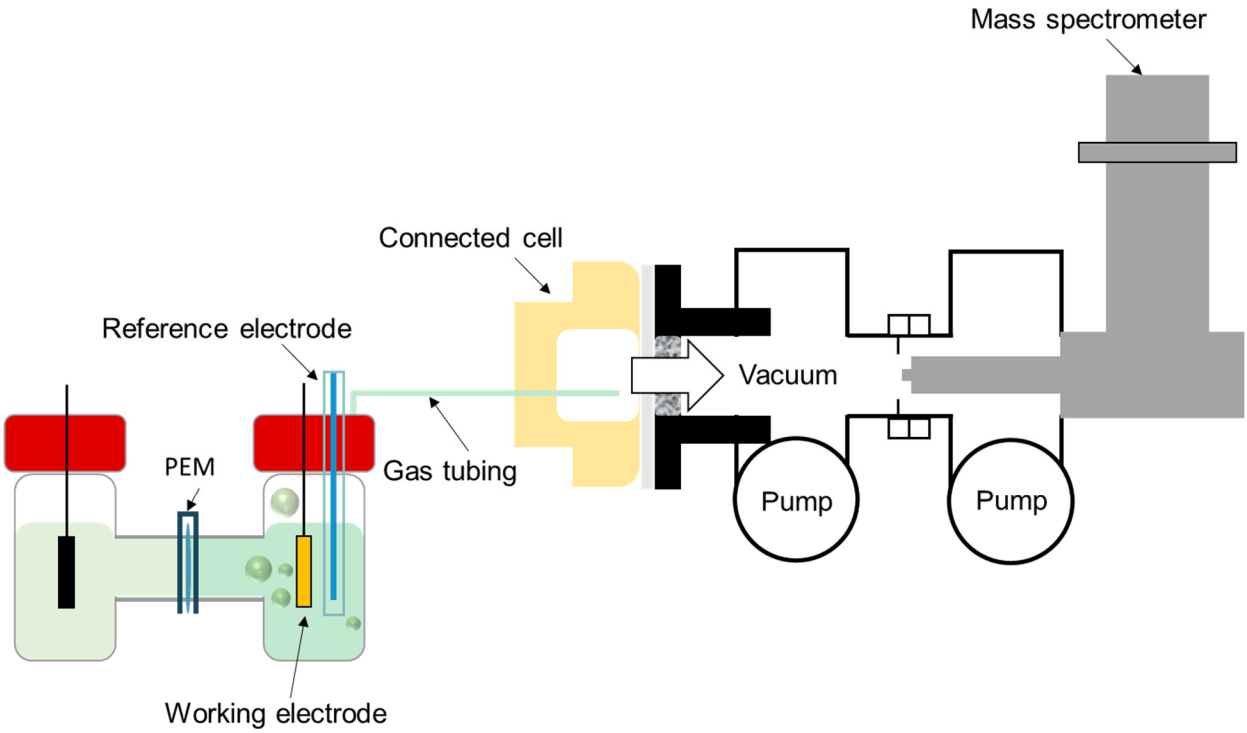

Fig. S13. Schematic illustrating the setup used for DEMS analysis. The electrolysis is conducted in the H-type cell and the effluent gas is channeled into a connected cell which is coupled to the mass spectrometer. The amount of effluent gas entering the mass spectrometer for analysis is controlled through a leak valve.

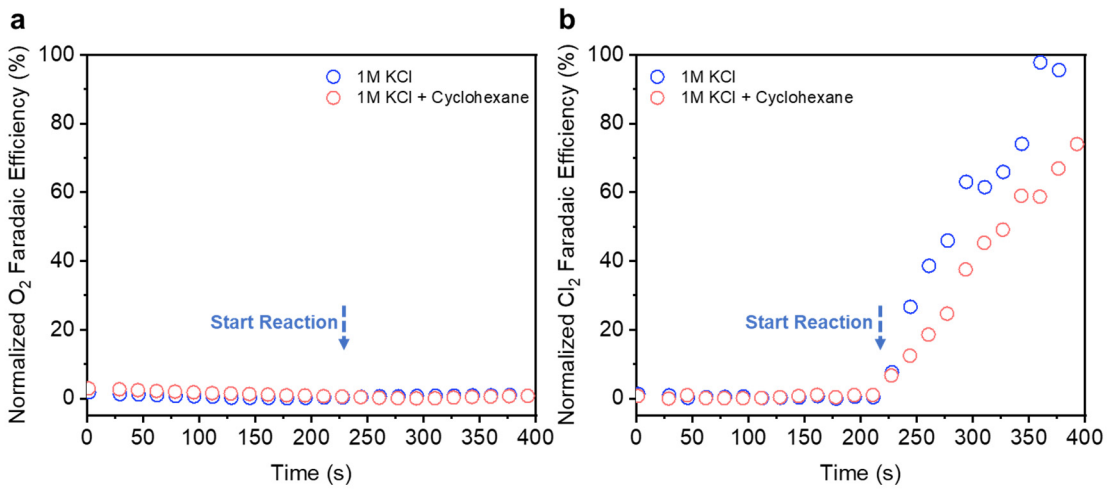

Fig. S14. Normalized Faradaic efficiency of (a) O_2 (m/z=32) and (b) Cl_2 (m/z=69.9) collected when different electrolytes are employed using C at a current of 400 mA.

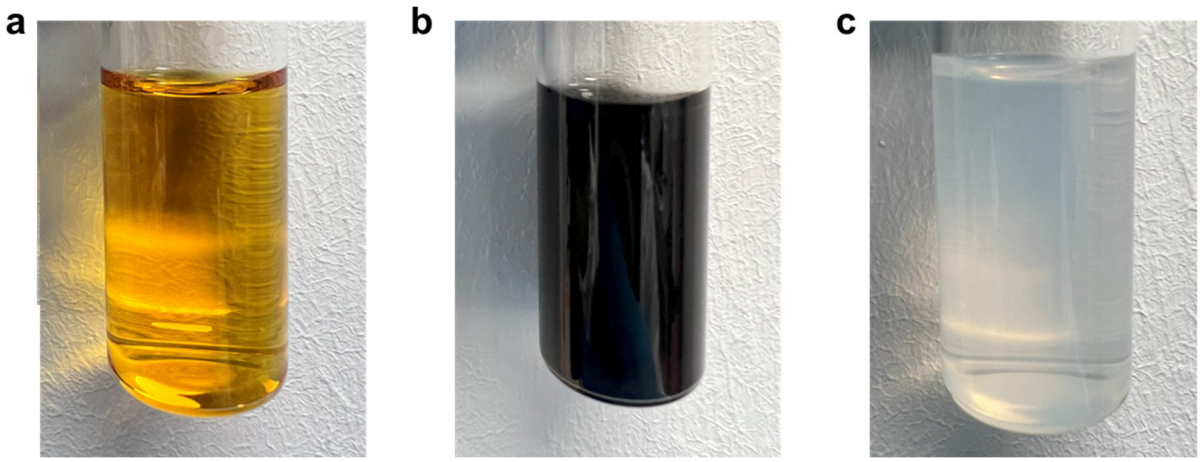

Fig. S15. (a) Digital photograph of the anolyte after addition of excess 10% KI solution. A brown coloration is observed due to oxidation of I^- to form I_2. (b) Digital photograph of the same anolyte after starch solution was added, forming a dark blue starch-iodine complex. (c) Digital photograph of the anolyte after titration with $Na_2S_2O_3$, yielding a clear colourless solution.

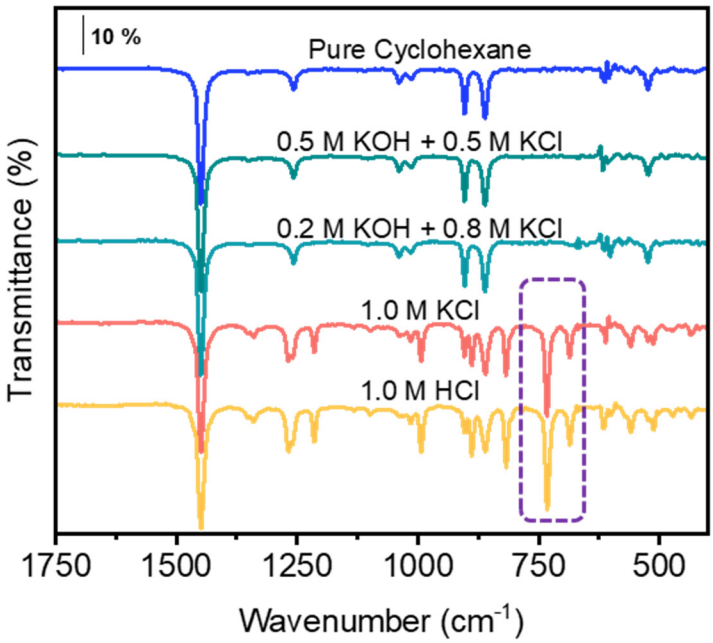

Fig. S16. FTIR spectroscopy of samples obtained under 800 mA in different electrolytes using IrO_x as the anode. We do not observe the presence of chlorocyclohexane formation under alkaline conditions.

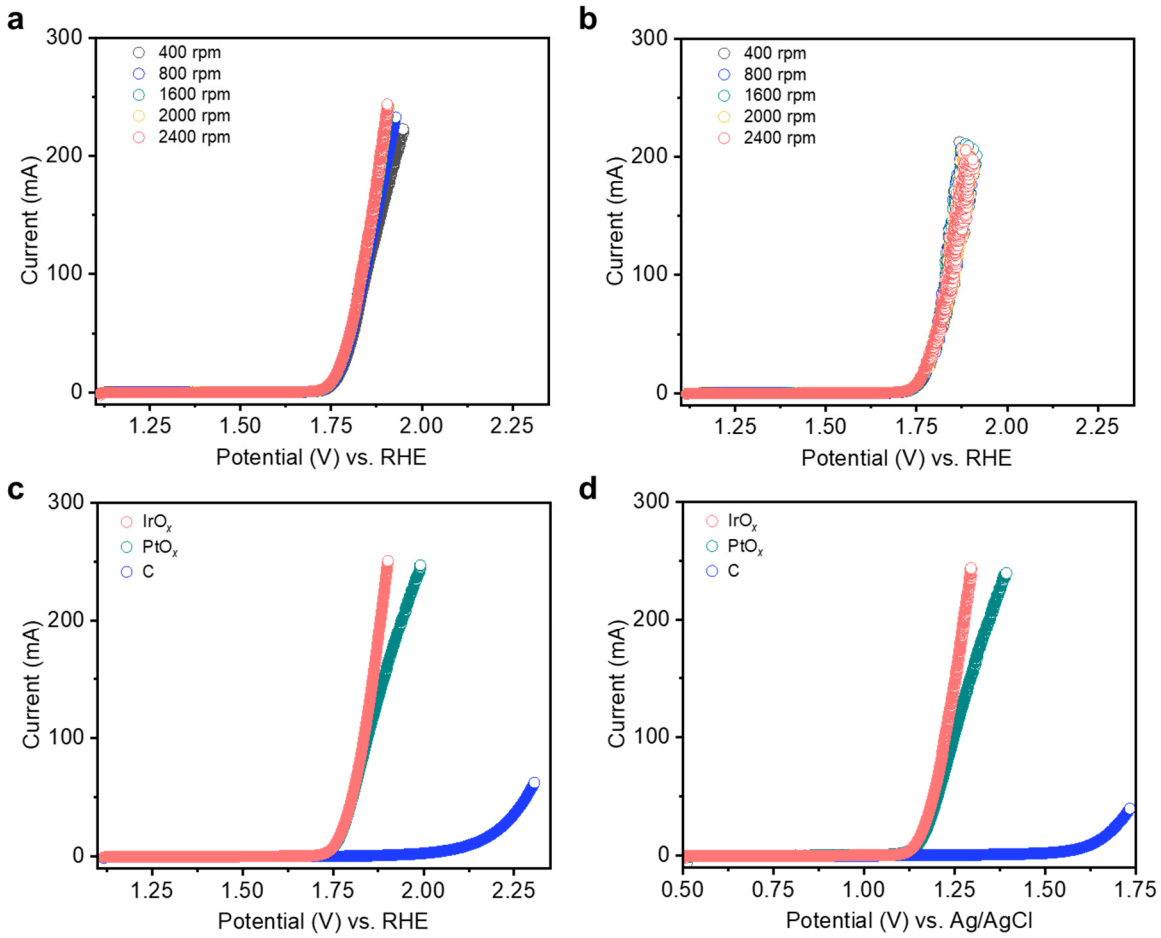

Fig. S17. LSV curves obtained with IrO_x electrode under different rotation speeds using (a) KCl and (b) KCl and cyclohexane mixture as the electrolyte. LSV curves obtained by different electrodes using (c) KCl and (d) KCl and cyclohexane mixture as the electrolyte under a rotation speed of 2400 rpm.

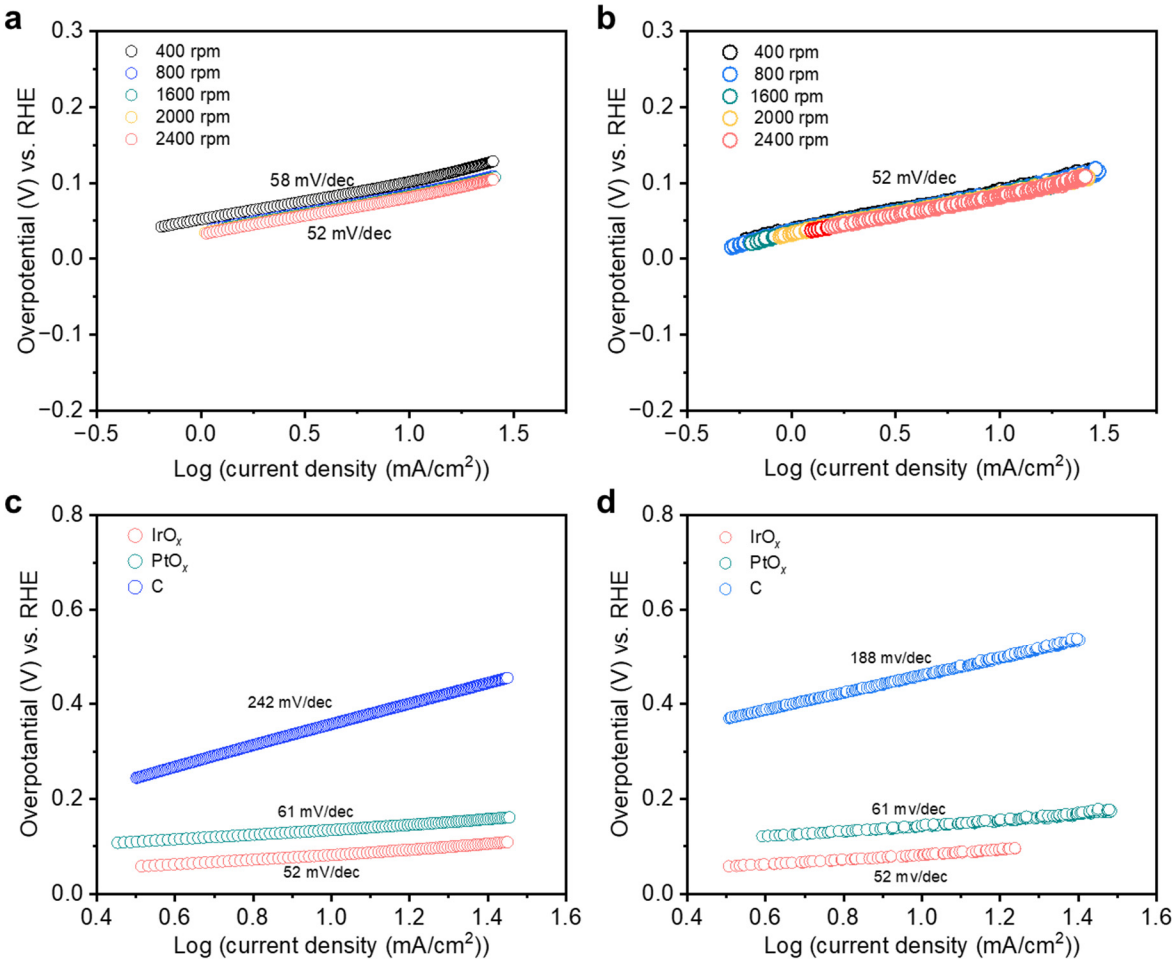

Fig. S18. Tafel slope obtained with IrO_x electrode under different rotation speeds using (a) KCl and (b) KCl and cyclohexane mixture as the electrolyte. Tafel slopes obtained by different electrodes using (c) KCl and (d) KCl and cyclohexane mixture as the electrolyte under a rotation speed of 2400 rpm.

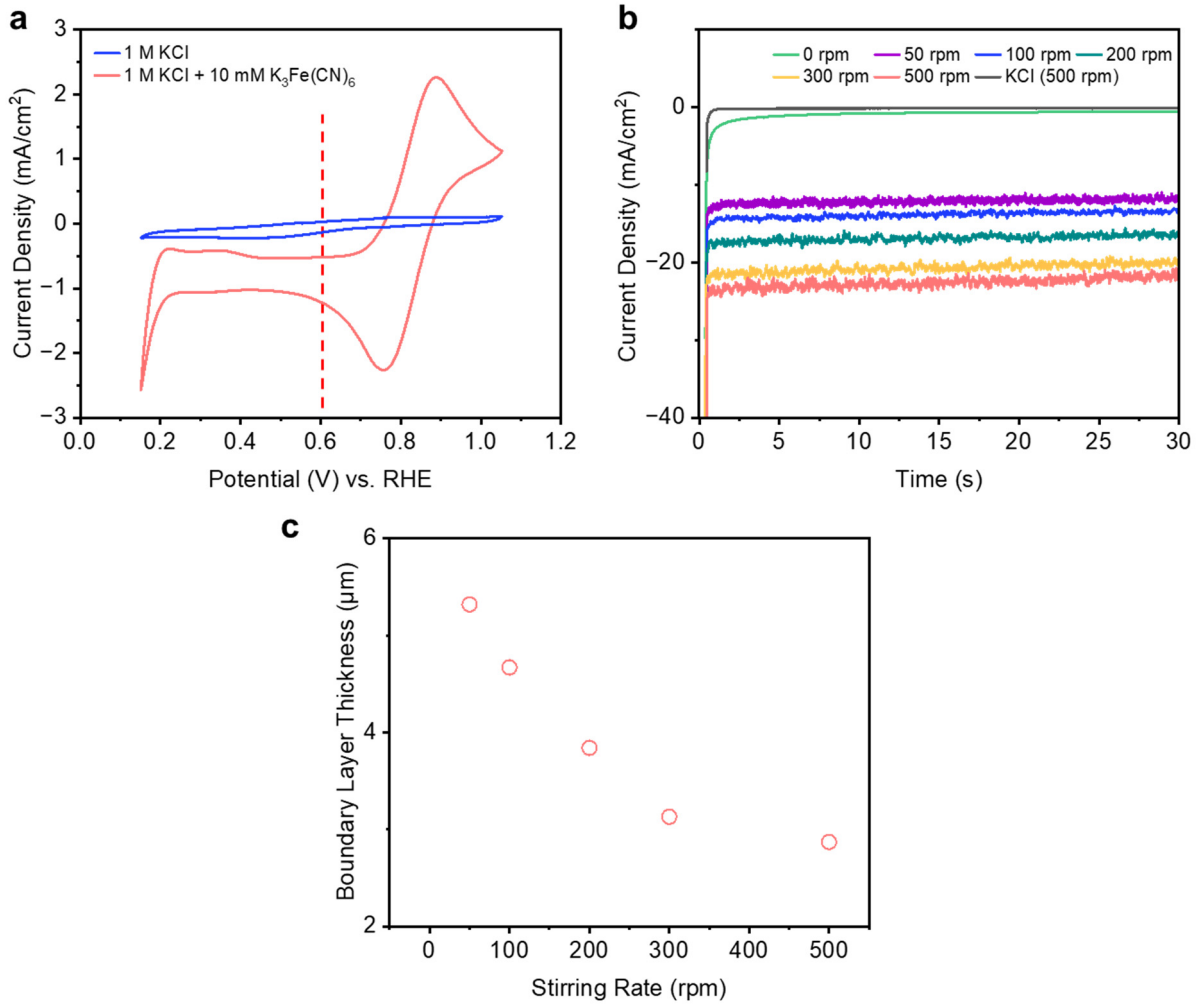

Fig. S19. Quantification of the hydrodynamic boundary layer thickness of the electrochemical cell. (a) Cyclic voltammograms obtained in 1 M KCl with and without the addition of 10 mM $K_3Fe(CN)_6$ (no stirring). The dotted red line indicates the potential used in the subsequent chronoamperometry experiments. (b) Chronoamperometry experiments utilized to measure the diffusion limited current density for ferricyanide reduction at various stirring rates. (c) Calculated hydrodynamic boundary layer thicknesses as a function of stirring rate.

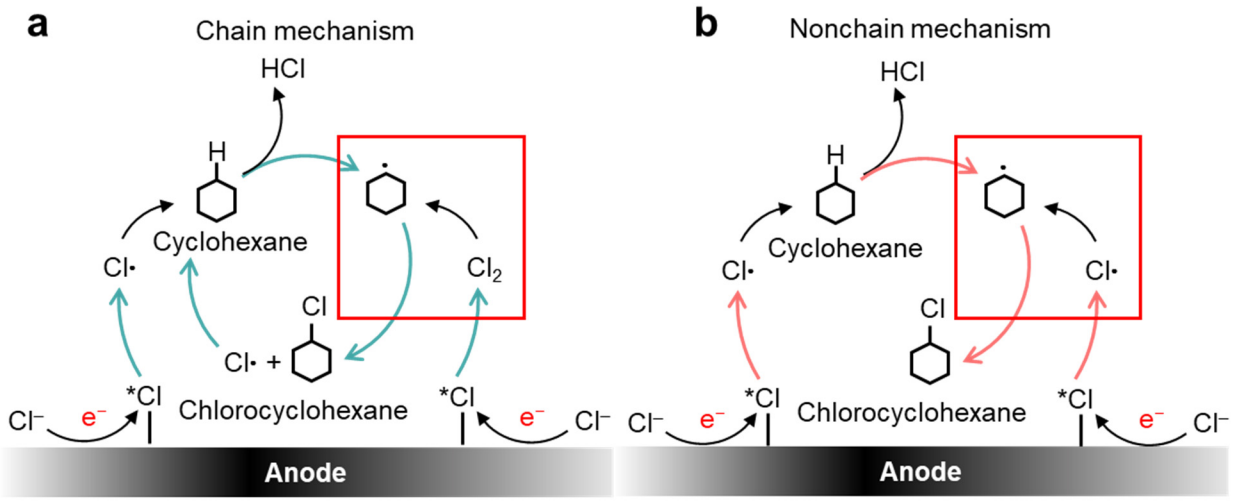

Fig. S20. Illustration of the chlorination of cyclohexane based on the: (a) chain mechanism and (b) nonchain mechanism.

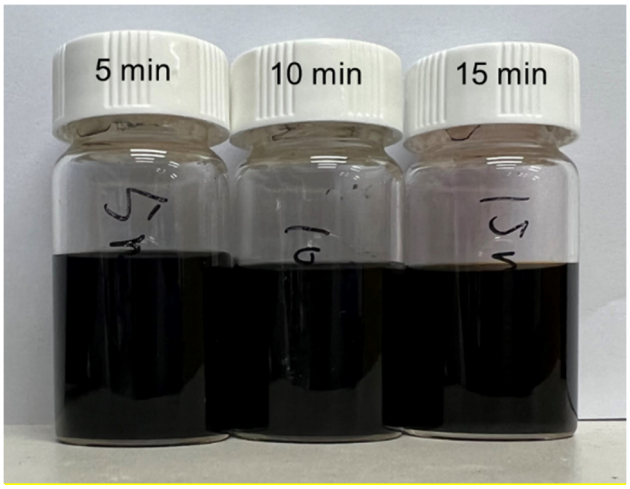

Fig. S21. Photographs of the pretreated electrolytes after the addition of KI and starch solution, which results in the formation of a dark blue starch-iodine complex. This procedure can be used to quantify the amount of Cl_2 in the electrolyte. These pretreated electrolytes were generated by performing the chlorine evolution reaction for 5, 10, or 15 min at 200 mA/cm^2 in 1 M HCl.

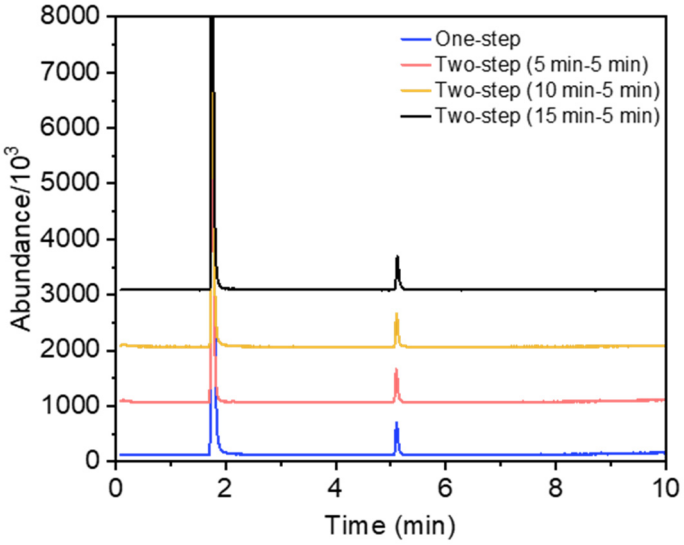

Fig. S22. Comparison of the GC-MS analysis results obtained under different conditions. 'One-step' represents the case in which cyclohexane was added to 1 M HCl and used as the electrolyte for electrolysis at 200 mA/cm^2 for 5 min. 'Two-step' represents the case in which we conducted electrolysis for 5, 10, or 15 mins in 1 M HCl at 200 mA/cm^2 (without cyclohexane) to introduce dissolved Cl_2 into the electrolyte. Following this, we added cyclohexane to these pretreated electrolytes and performed another 5 min of electrolysis at 200 mA/cm^2.

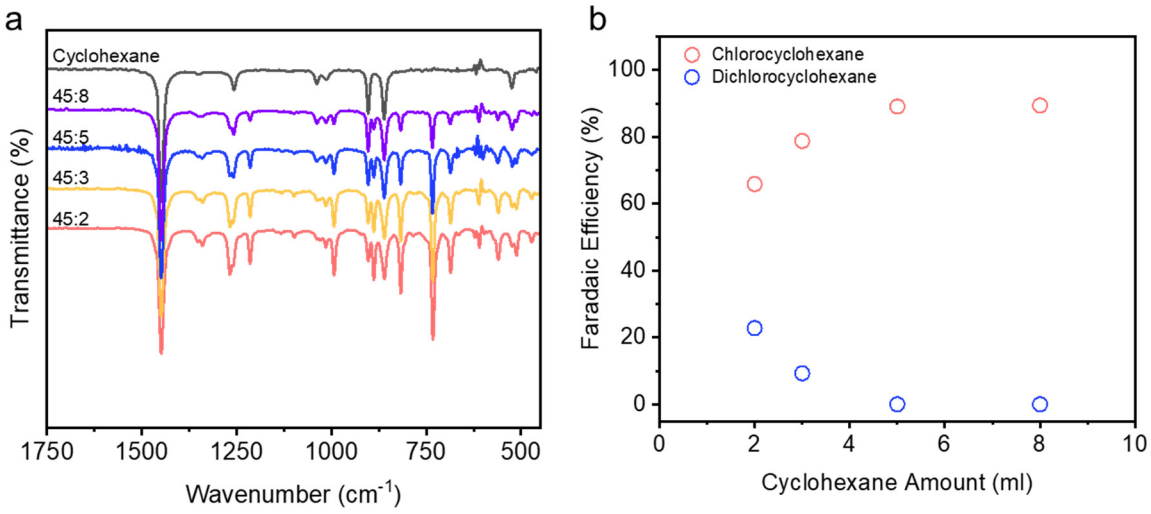

Fig. S23. (a) FTIR spectroscopy of samples obtained using various amounts of cyclohexane in the electrolyte at a current of 1000 mA with an electrolysis duration of 30 min. (b) FE towards chlorocyclohexane and dichlorocyclohexane obtained with different volumes of cyclohexane in the electrolyte at 1000 mA and an electrolysis duration of 30 min.

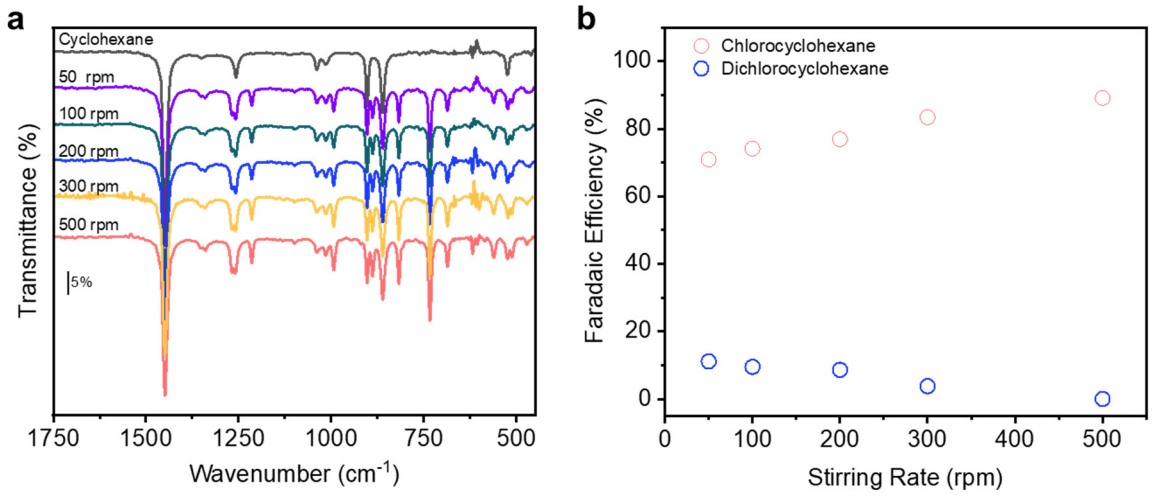

Fig. S24. (a) FTIR spectroscopy results and (b) FE towards chlorocyclohexane and dichlorocyclohexane of samples obtained at different stirring rates with a current of 1000 mA for IrO_x based catalyst for a duration of 30 min.

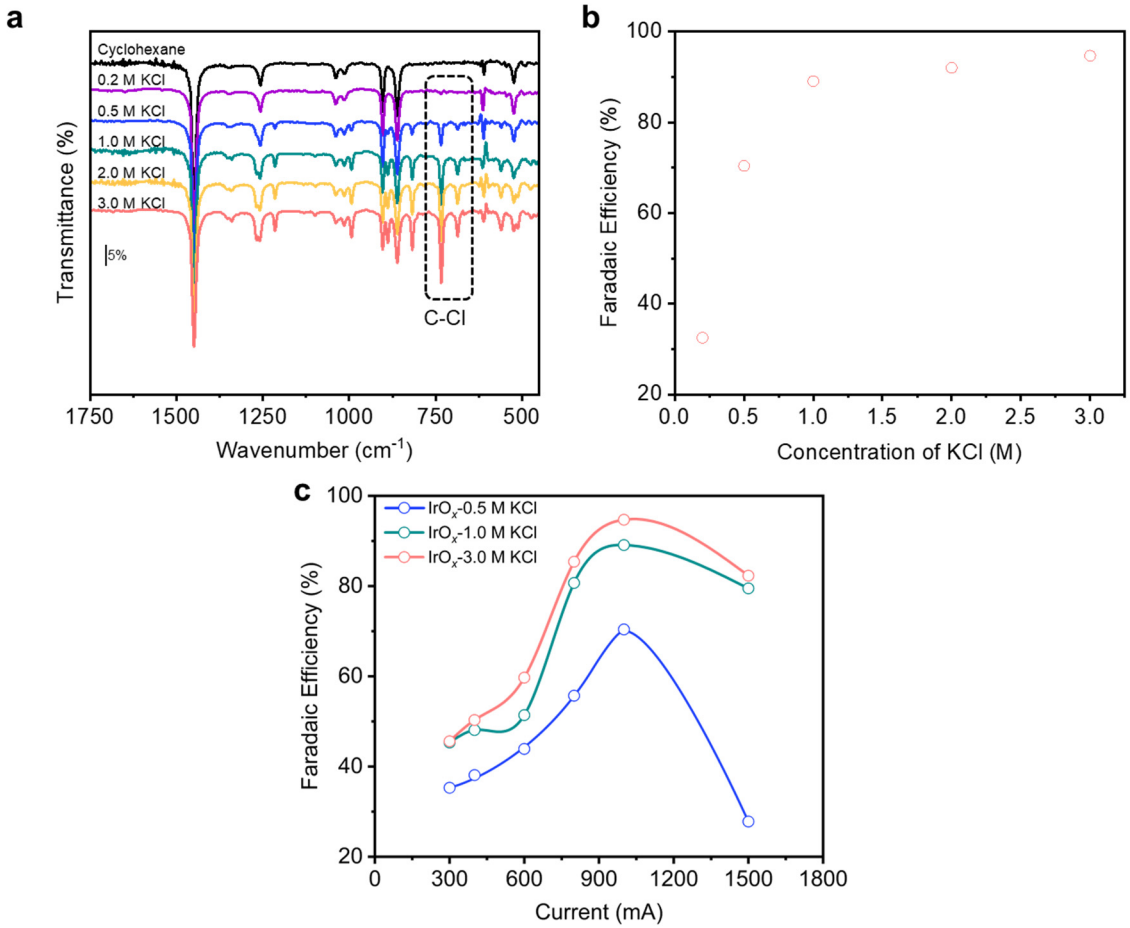

Fig. S25. Influence of the KCl concentration on the reaction. (a) FTIR spectroscopy of samples obtained with various KCl concentrations using IrO_x as the electrode using a current of 1000 mA. (b) Faradaic efficiency of chlorocyclohexane obtained with various concentrations of KCl using a current of 1000 mA and IrO_x as the electrode. (c) FE towards chlorocyclohexane obtained under various KCl concentrations and applied currents using IrO_x as the electrode.

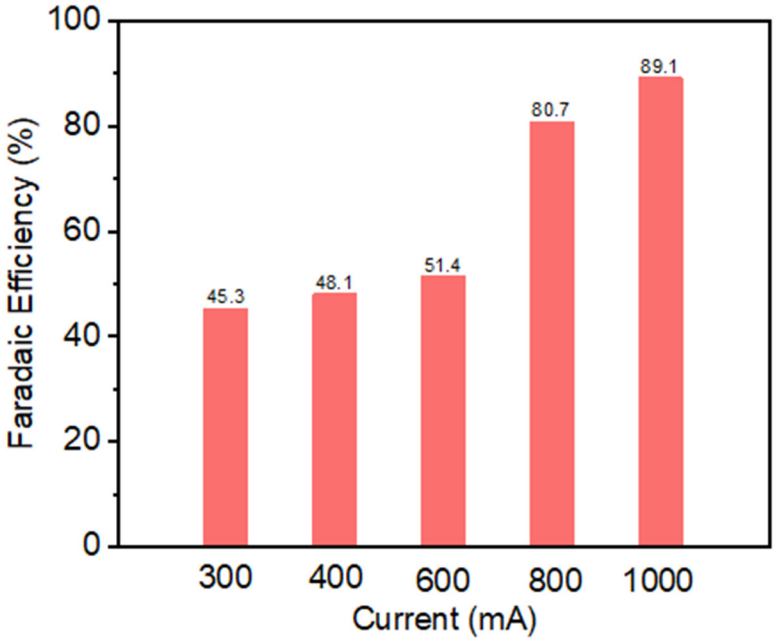

Fig. S26. FE towards chlorocyclohexane under different applied currents for the IrO_x anode.

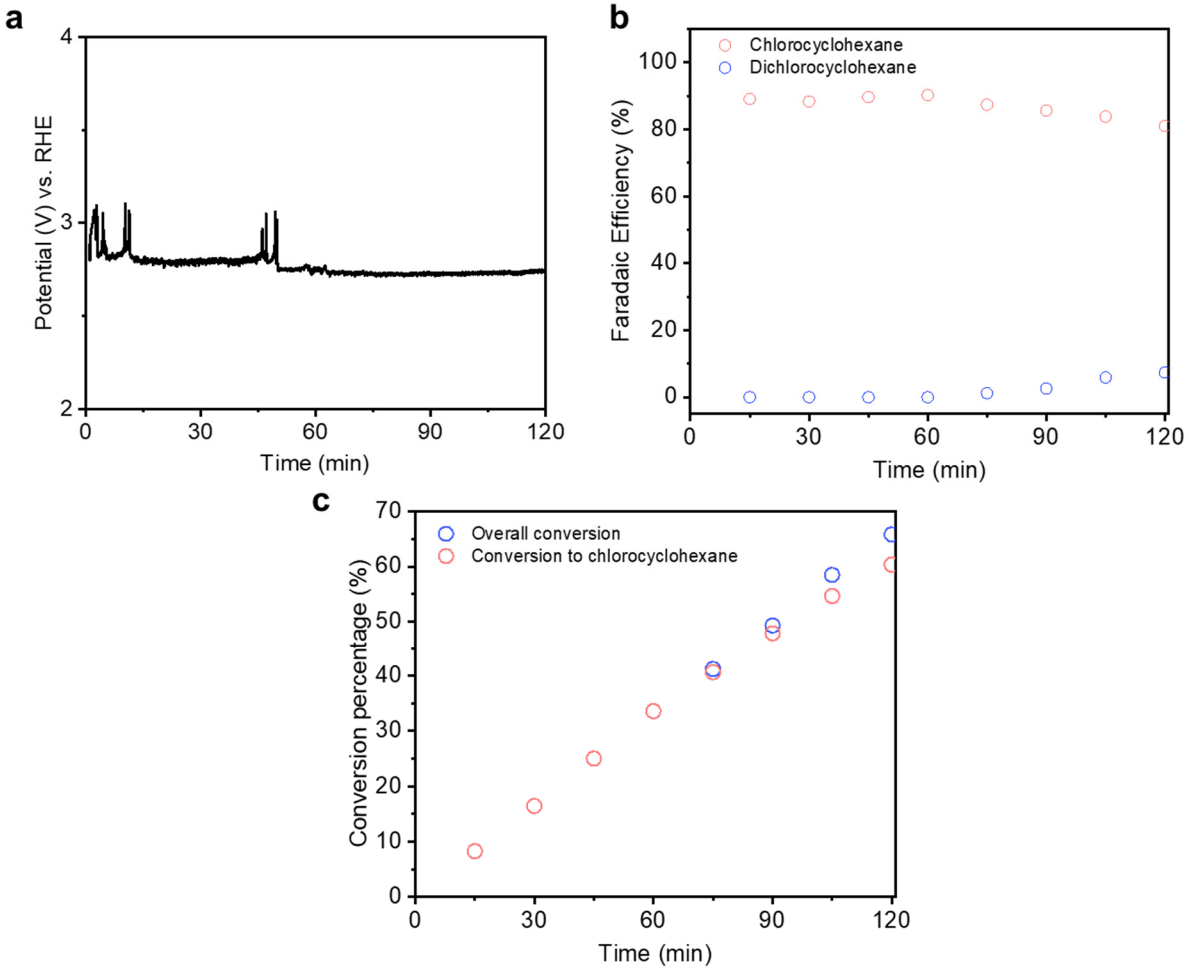

Fig. S27. (a) Applied potential and (b) FE towards chlorocyclohexane and dichlorocyclohexane at a current of 1000 mA over a 2 h period with IrO_x as the electrode. 5 ml cyclohexane and 45 ml KCl was used as the electrolyte. (c) The cyclohexane conversion percentage over 2 h.

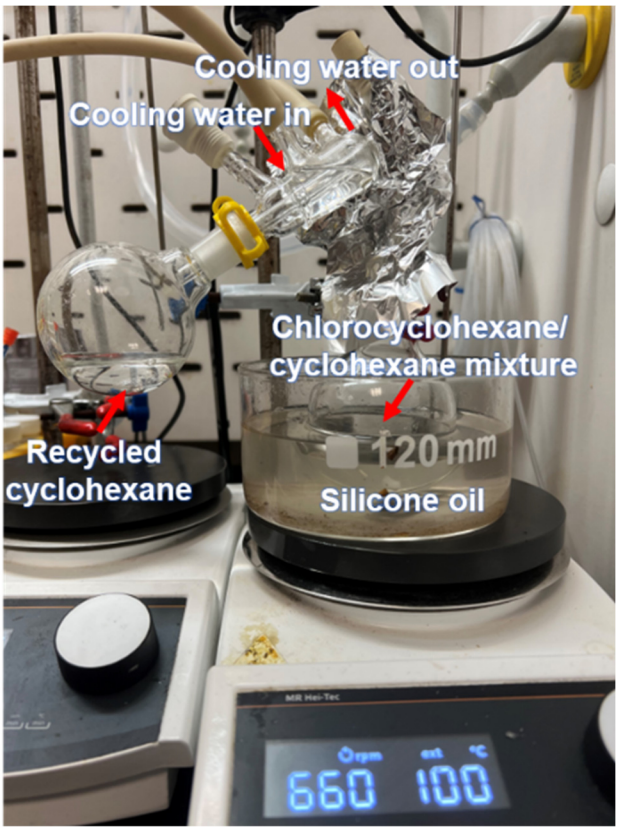

Fig. S28. Picture taken of the distillation setup used for recycling the cyclohexane from chlorocyclohexane/cyclohexane mixture. The heating temperature was set to 100 °C to remove the lower boiling point cyclohexane (81 °C) from the higher boiling point chlorocyclohexane (142 °C). The recycled cyclohexane was then used for another round of chlorination.

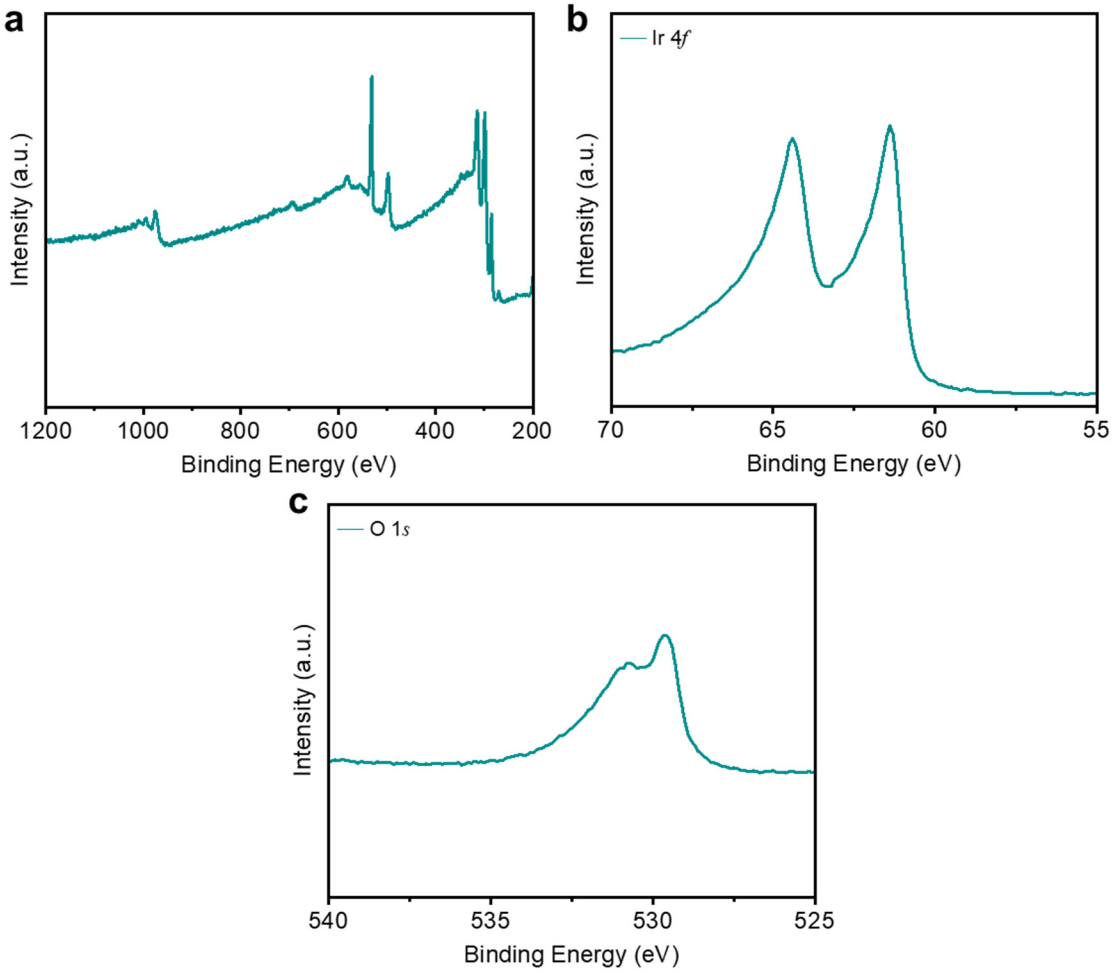

Fig. S29. XPS measurements of IrO_x before electrolysis experiments. (a) survey spectra, (b) Ir 4*f* narrow scan and (c) O 1*s* narrow scan.

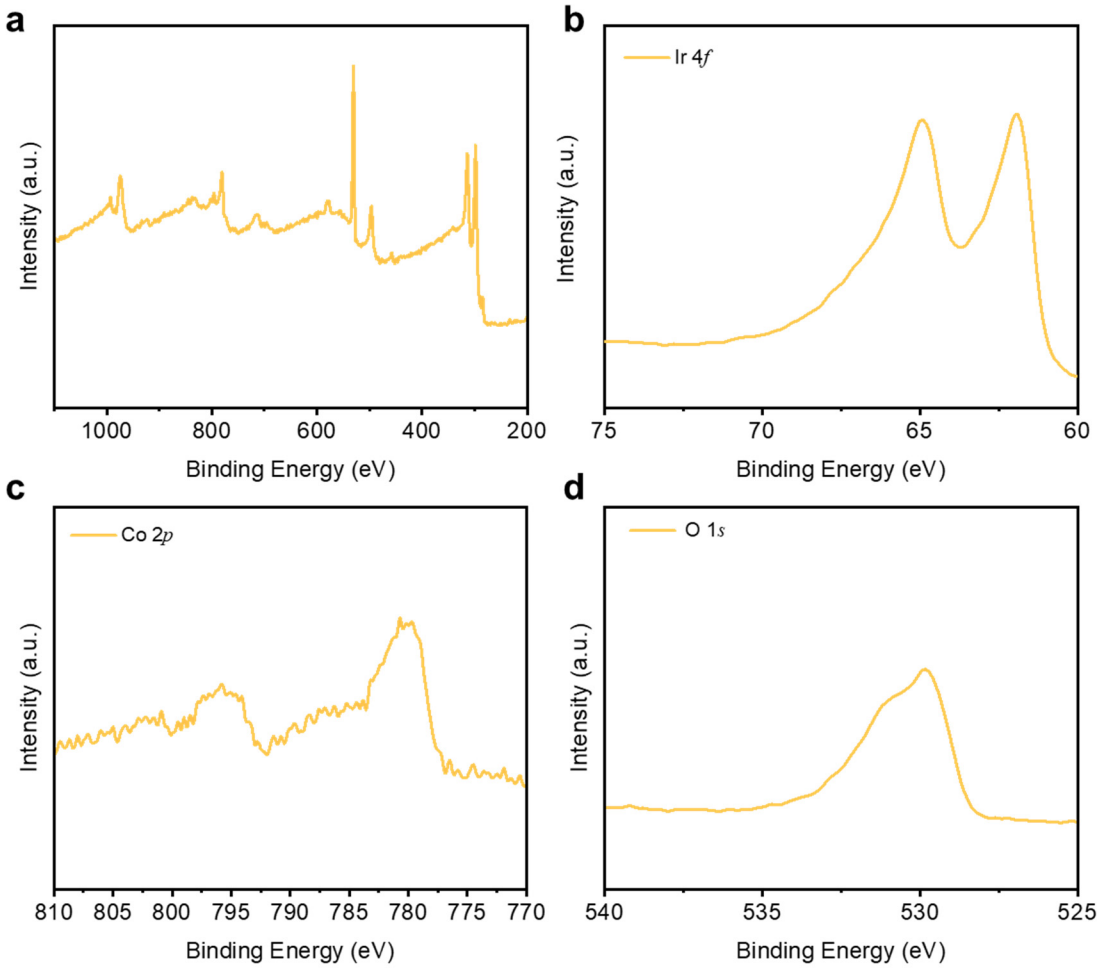

Fig. S30. XPS measurements of Co/IrO_x before electrolysis experiments. (a) survey spectra, (b) Ir 4*f* narrow scan and (c) Co 2*p* narrow scan and (d) O 1*s* narrow scan.

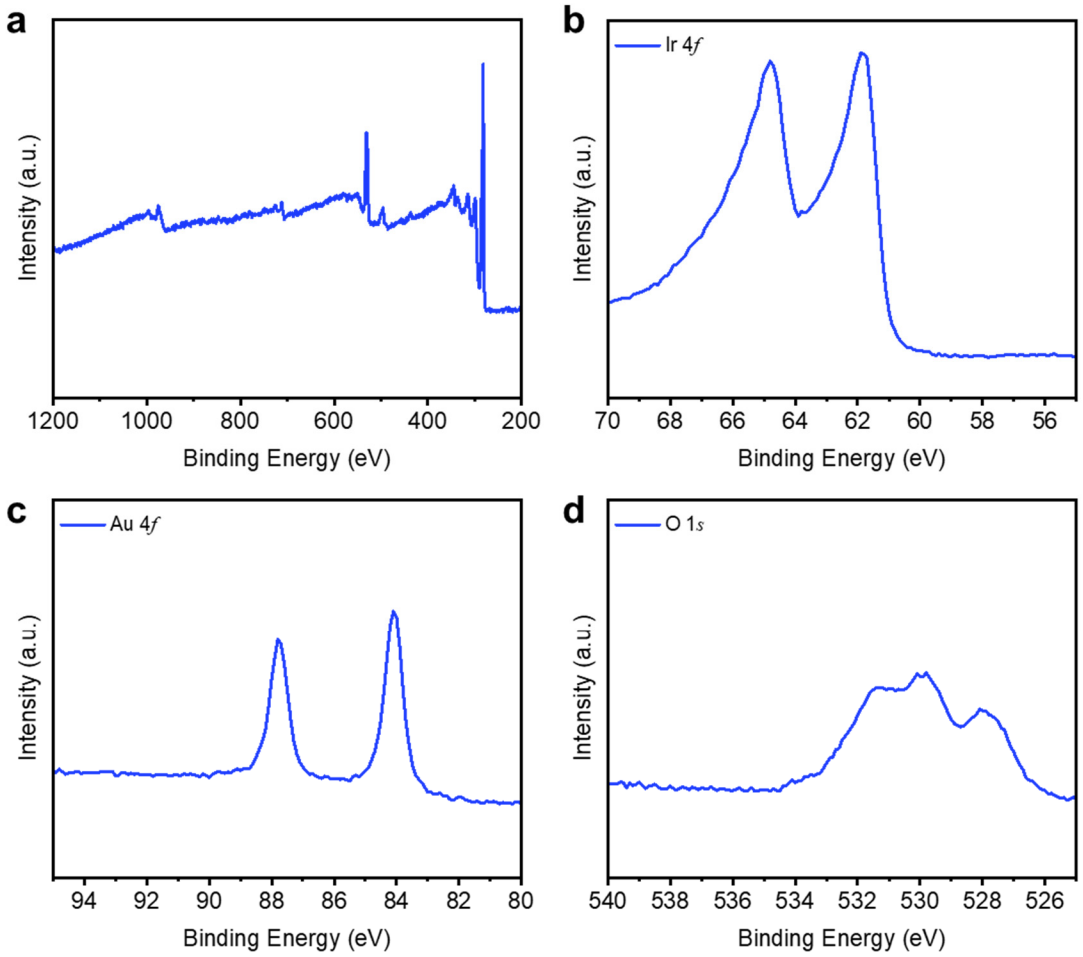

Fig. S31. XPS measurements of Au/IrO_x before electrolysis experiments. (a) survey spectra, (b) Ir 4*f* narrow scan and (c) Au 4*f* narrow scan and (d) O 1*s* narrow scan.

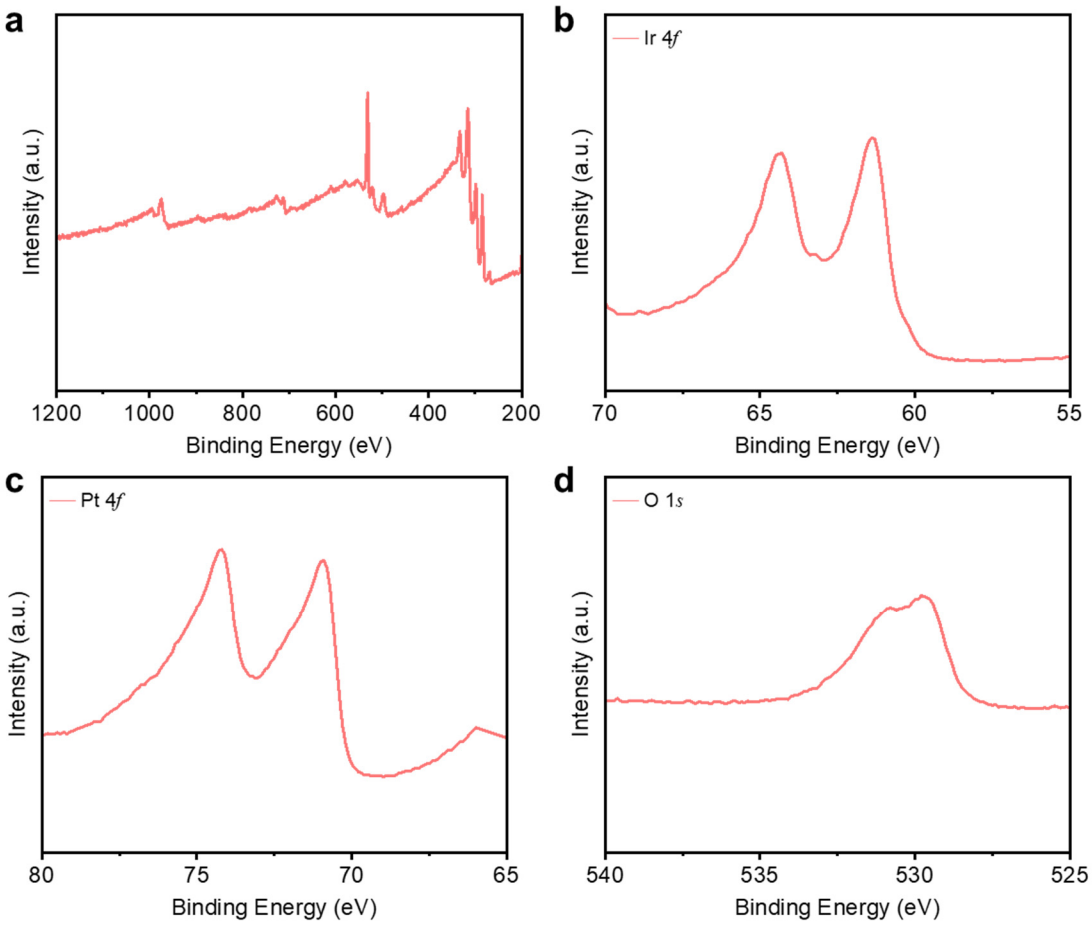

Fig. S32. XPS measurements of Pt/IrO_x before electrolysis experiments. (a) survey spectra, (b) Ir 4*f* narrow scan and (c) Pt 4*f* narrow scan and (d) O 1*s* narrow scan.

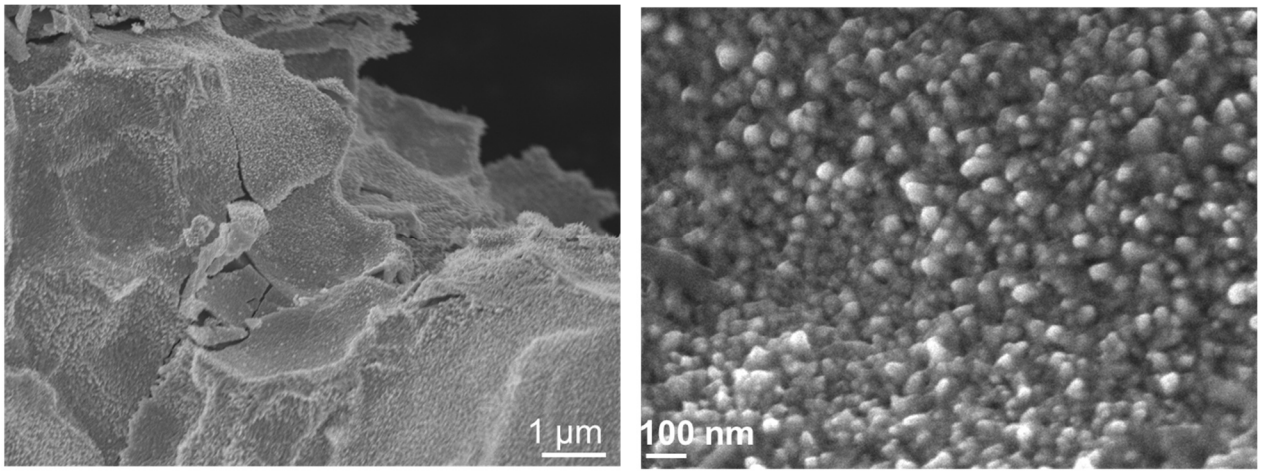

Fig. S33. SEM images of the IrO_x anode.

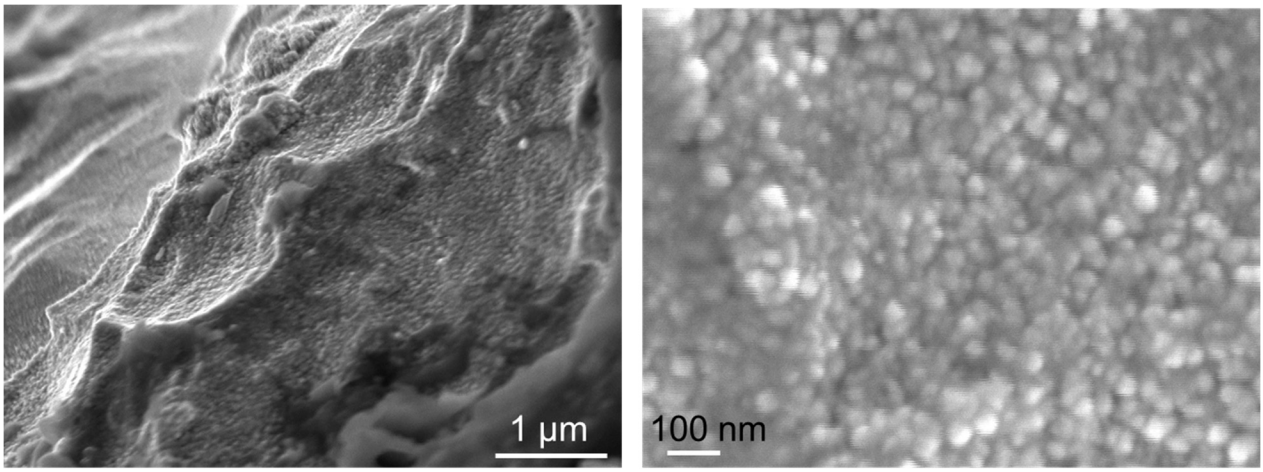

Fig. S34. SEM images of the Co/IrO_x anode.

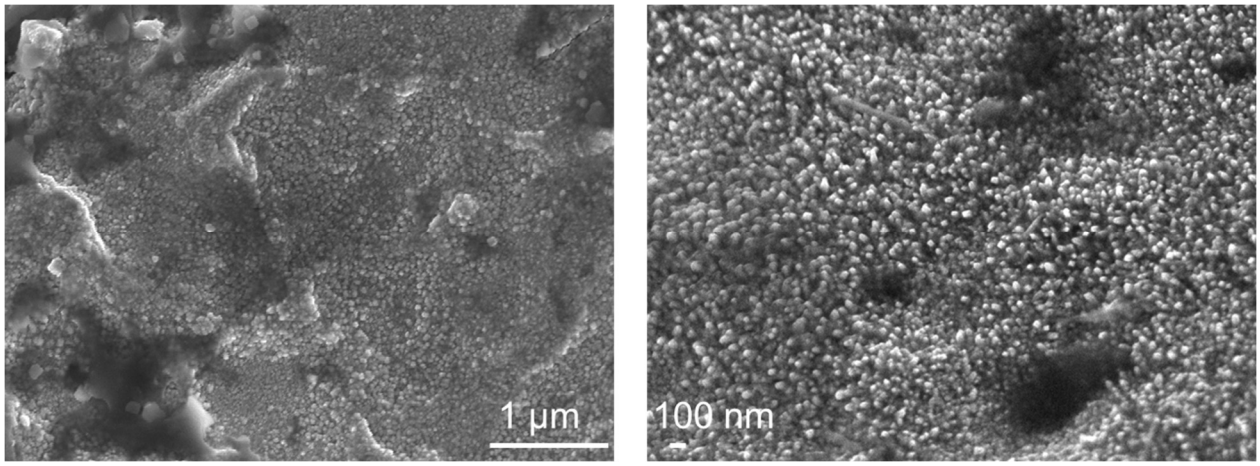

Fig. S35. SEM images of the Au/IrO_x anode.

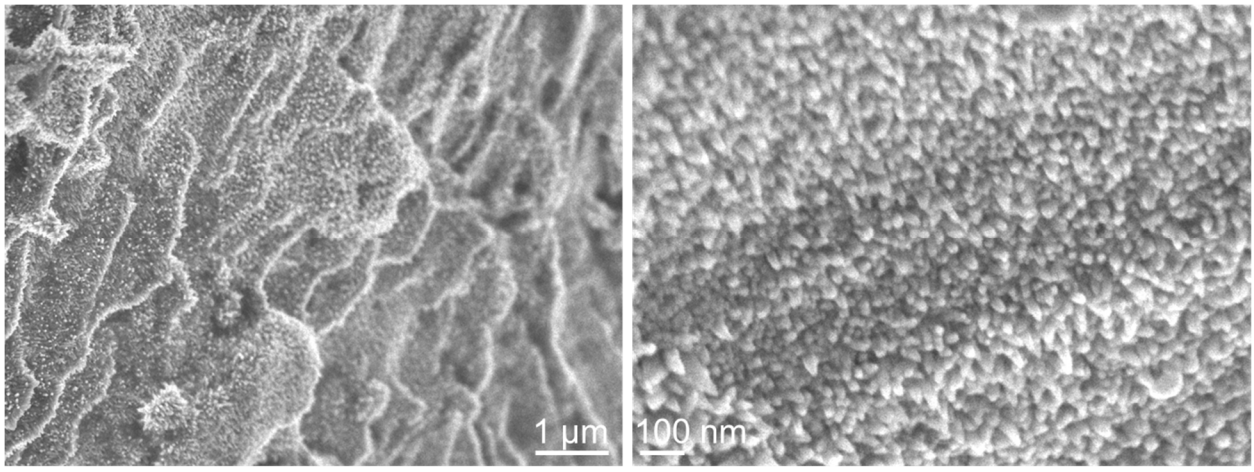

Fig. S36. SEM images of the Pt/IrO_x anode.

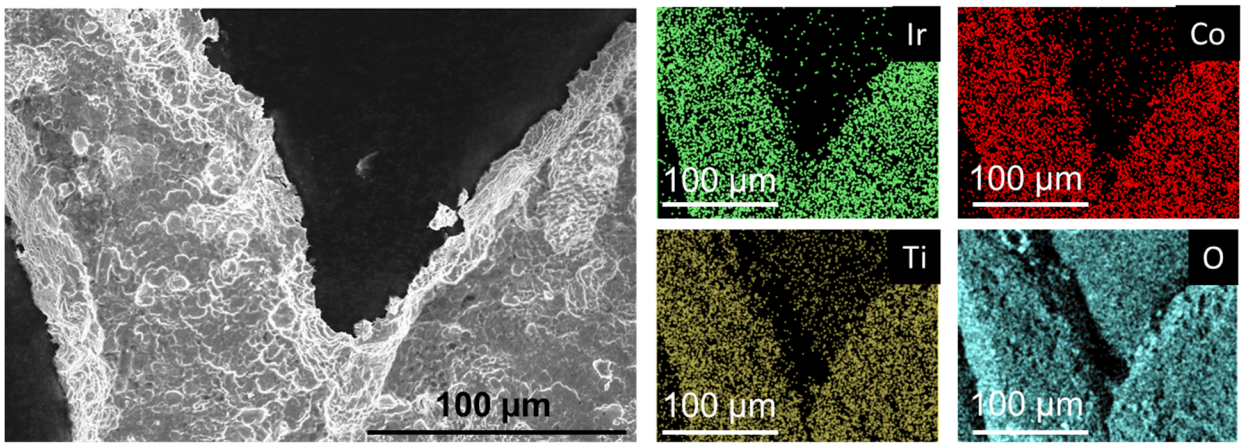

Fig. S37. SEM EDS mapping of the Co/IrO_x anode.

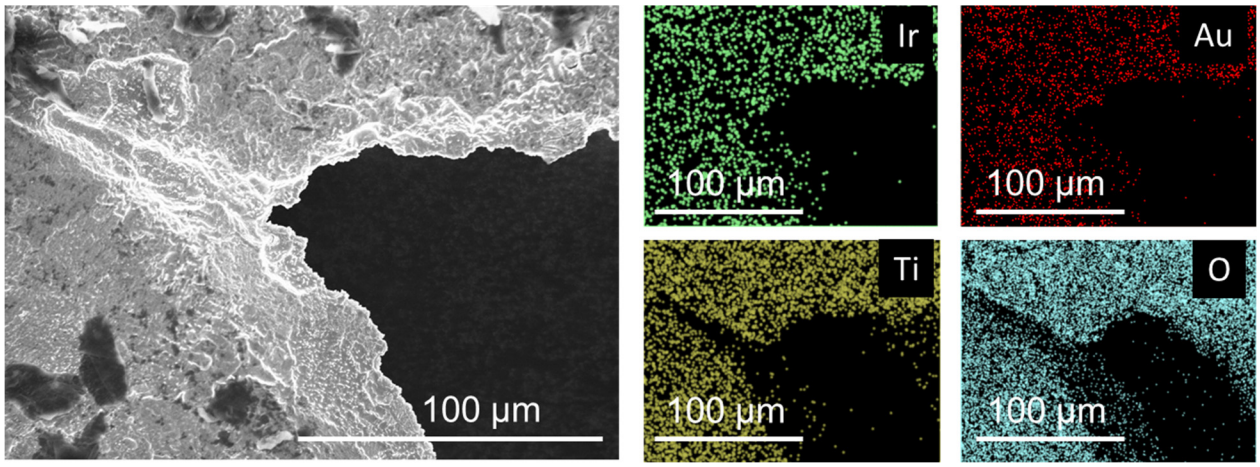

Fig. S38. SEM EDS mapping of the Au/IrO_x anode.

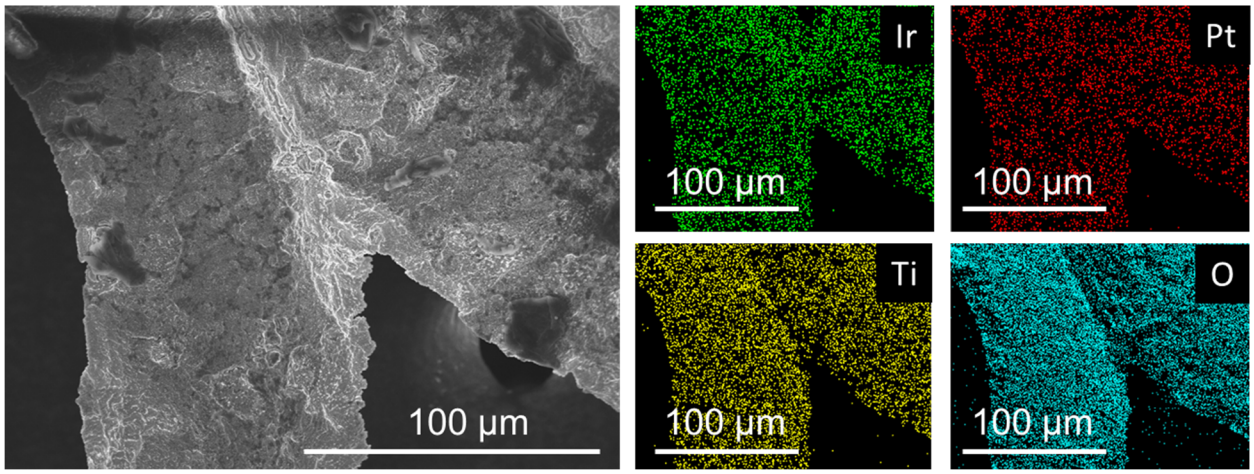

Fig. S39. SEM EDS mapping of the Pt/IrO_x anode.

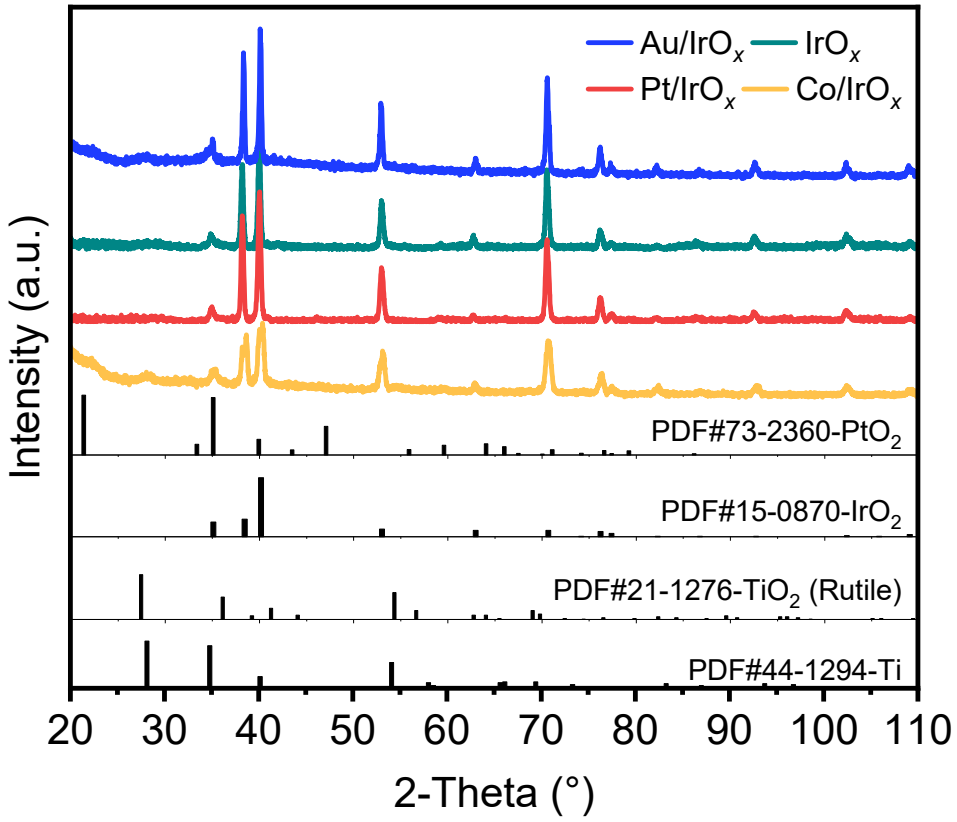

Fig. S40. XRD analysis of the different IrO_x-based catalysts, with standard cards shown for reference and comparison.

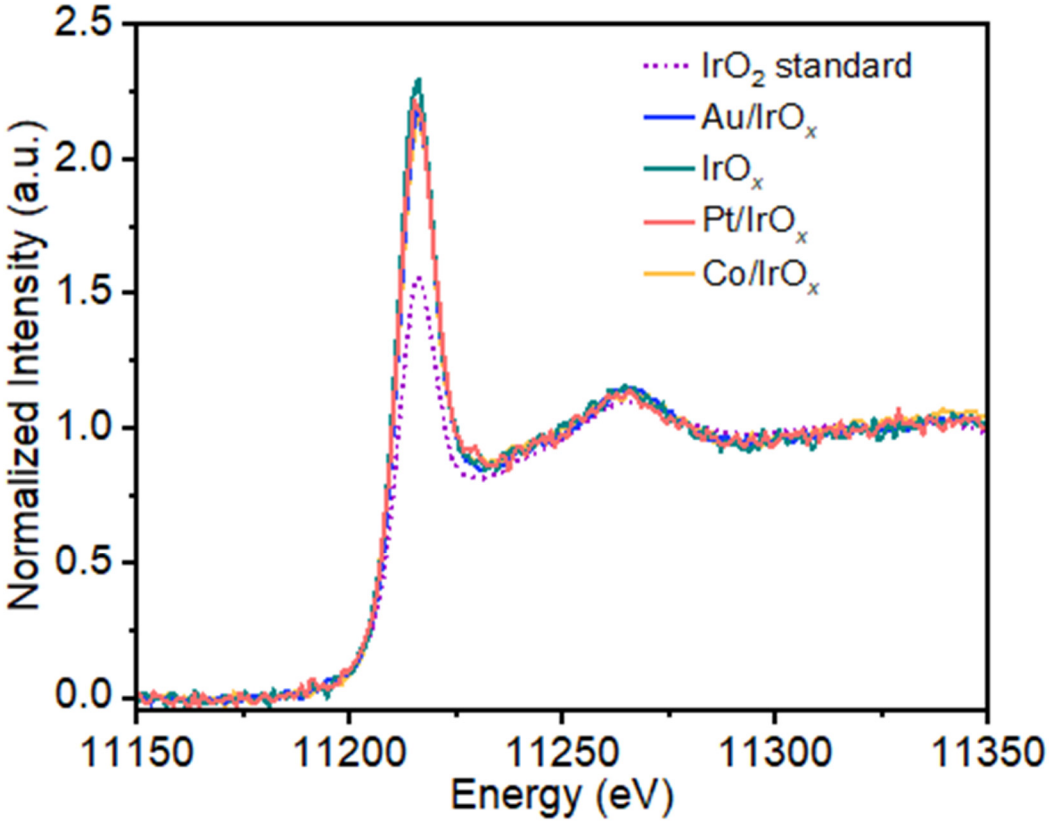

Fig. S41. Ir L_3-edge XANES spectra of different IrO_x-based catalysts.

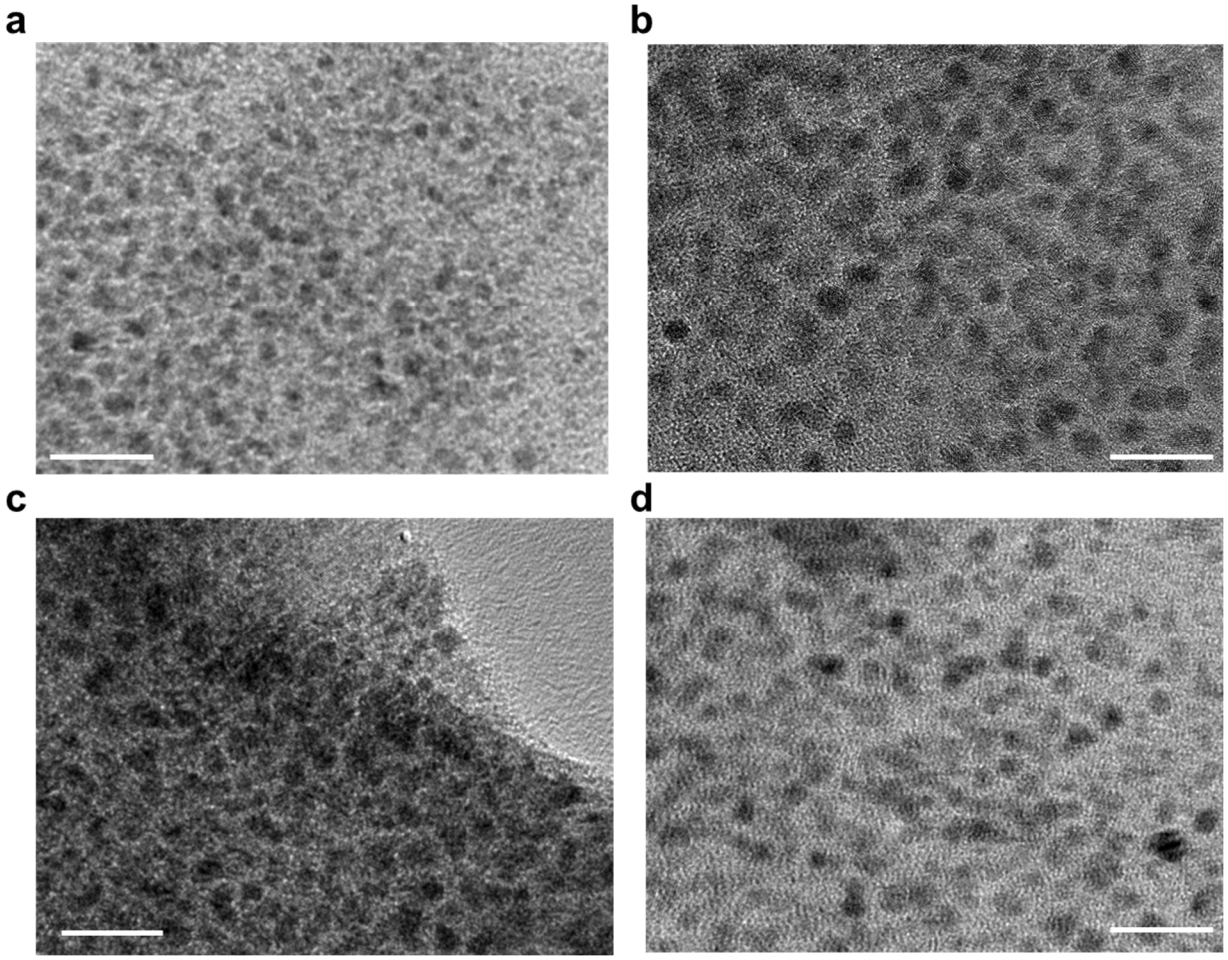

Fig. S42. TEM images of (a) IrO_x. (b) Pt/IrO_x. (c) Au/IrO_x. (d) Co/IrO_x. In all cases, the scale bars represent 10 nm.

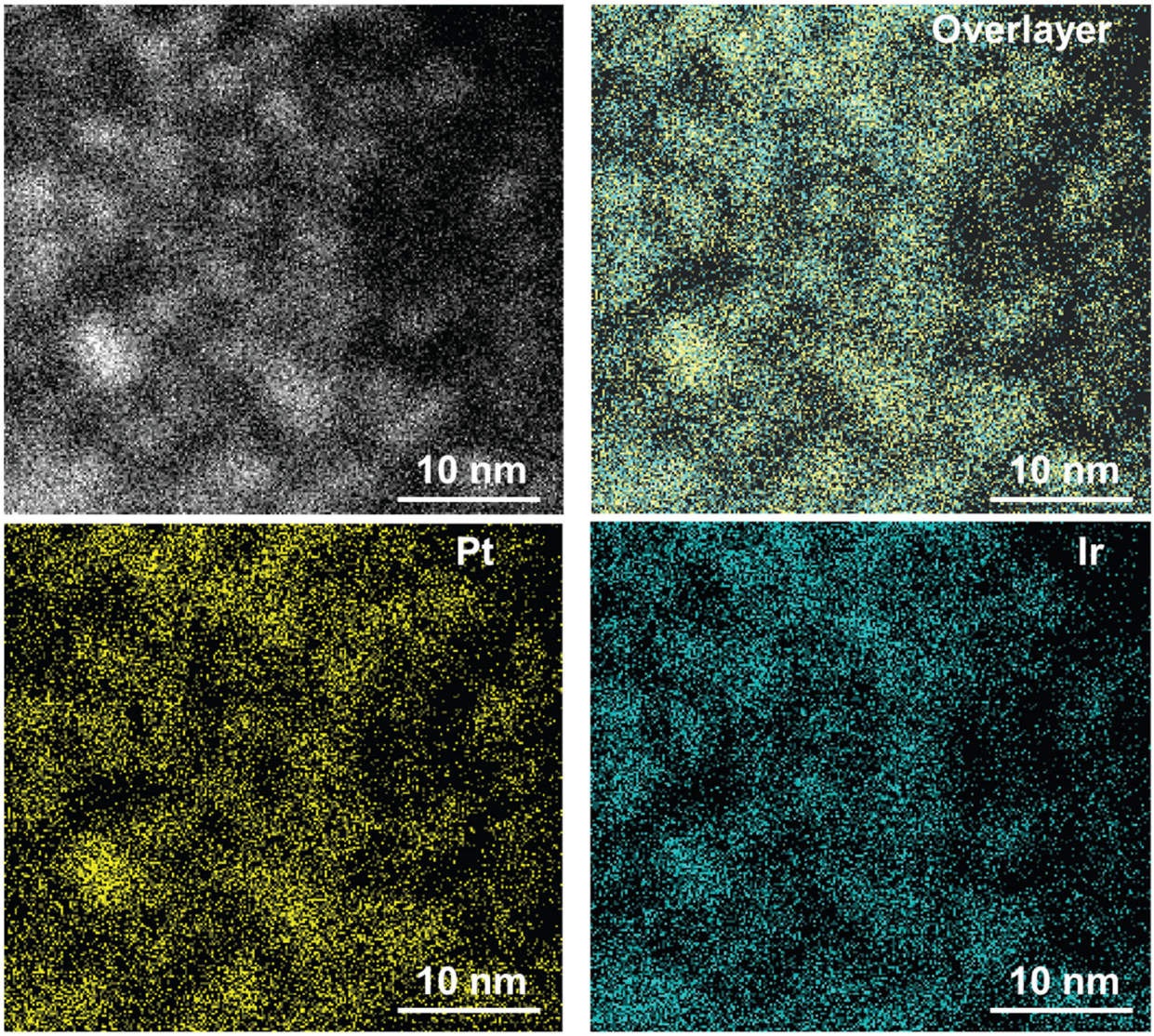

Fig. S43. TEM EDS mapping of the Pt/IrO_x anode.

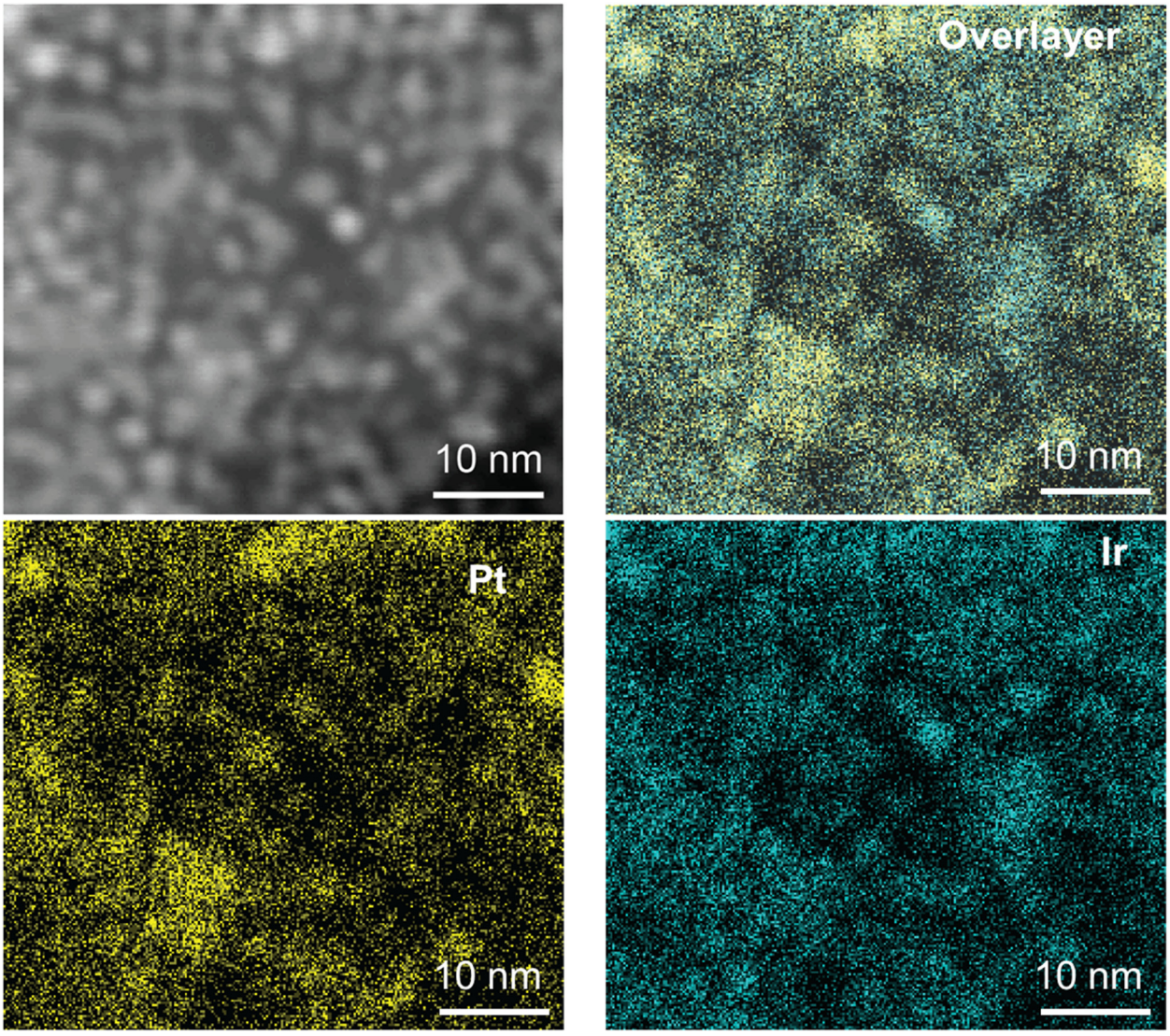

Fig. S44. TEM EDS mapping of the Pt/IrO_x anode.

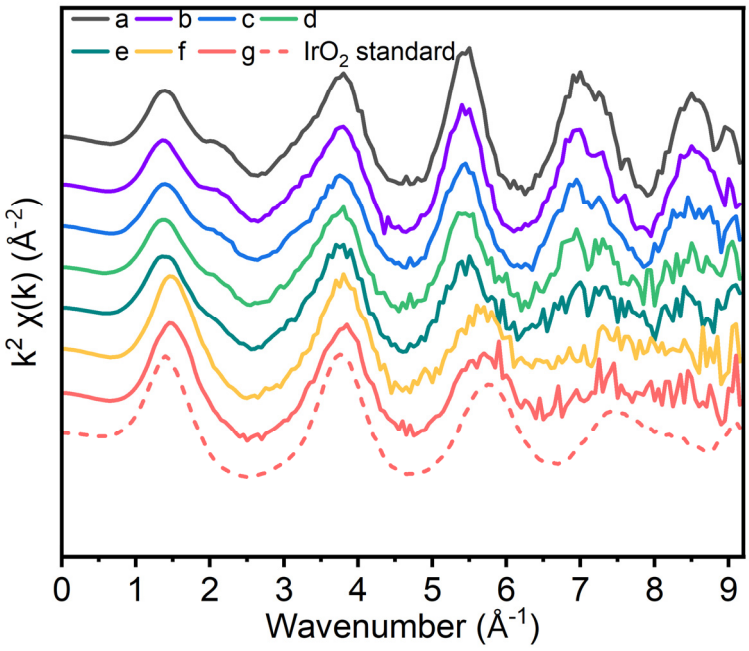

Fig. S45. The *k*-space XAS spectra of the thermal annealing process from stage a to g.

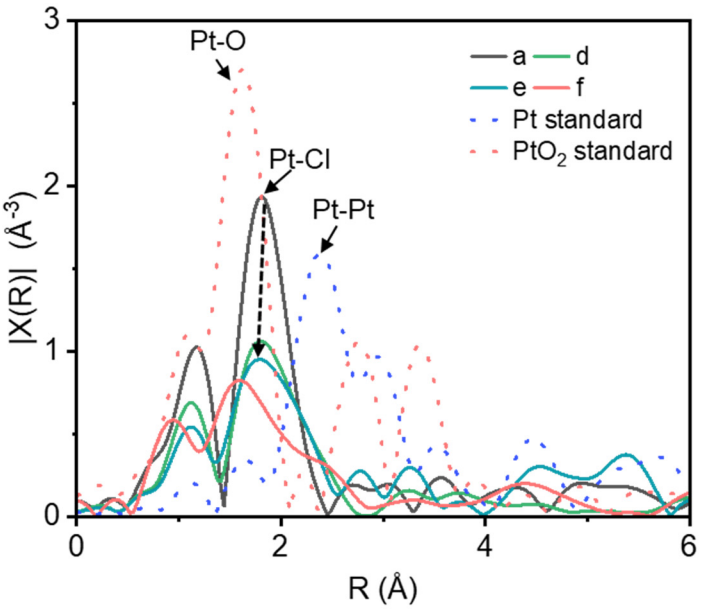

Fig. S46. Pt-L_3 edge Fourier-transform EXAFS spectra of the thermal annealing process for the synthesis of Pt/IrO_x from stage a to g.

Table S1. Chlorocyclohexane FE and applied potential at various applied currents with IrO_x.

Current (mA)	Faradaic Efficiency (%)	Potential (V) vs. RHE
300	45.3	2.1
400	48.1	2.19
600	51.4	2.37
800	80.7	2.55
1000	89.1	2.82

Table S2. Chlorocyclohexane FE and applied potential at various applied currents with Co/IrO_x.

Current (mA)	Faradaic Efficiency (%)	Potential (V) vs. RHE
300	37	2
400	68.4	2.05
600	82.6	2.18
800	78.3	2.29
1000	70.8	2.45

Table S3. Chlorocyclohexane FE and applied potential at various applied currents with Au/IrO_x.

Current (mA)	Faradaic Efficiency (%)	Potential (V) vs. RHE
300	22.1	2.18
400	45.9	2.32
600	46.1	2.55
800	63.6	2.77
1000	77.5	3.04

Table S4. Chlorocyclohexane FE and applied potential at various applied currents with Pt/IrO_x.

Current (mA)	Faradaic Efficiency (%)	Potential (V) vs. Ag/AgCl
300	52.9	2.01
400	61.2	2.1
600	67.5	2.29
800	88.5	2.46
1000	95.2	2.64

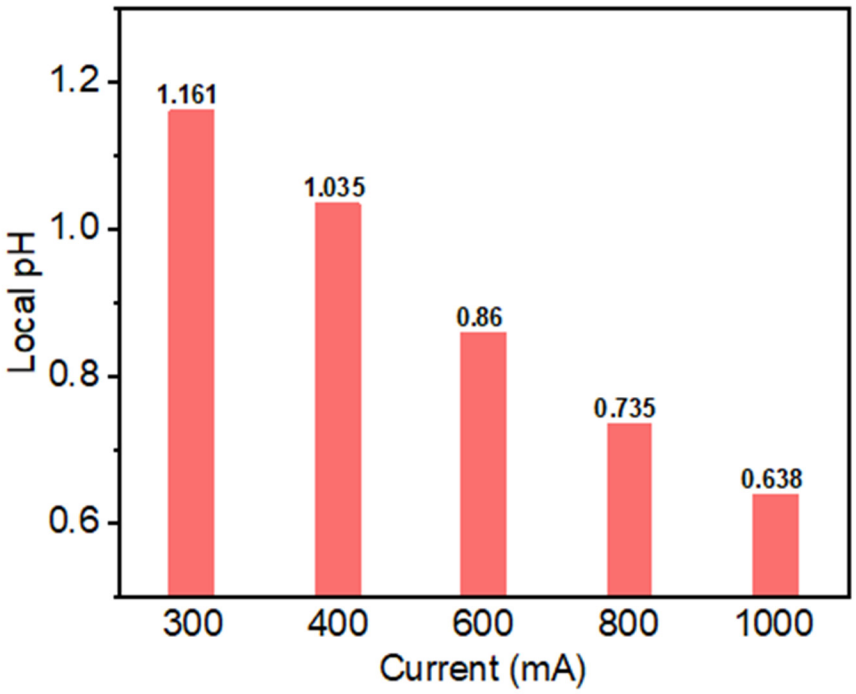

Fig. S47. Calculated local pH at different current densities for the Co/IrO_x anode.

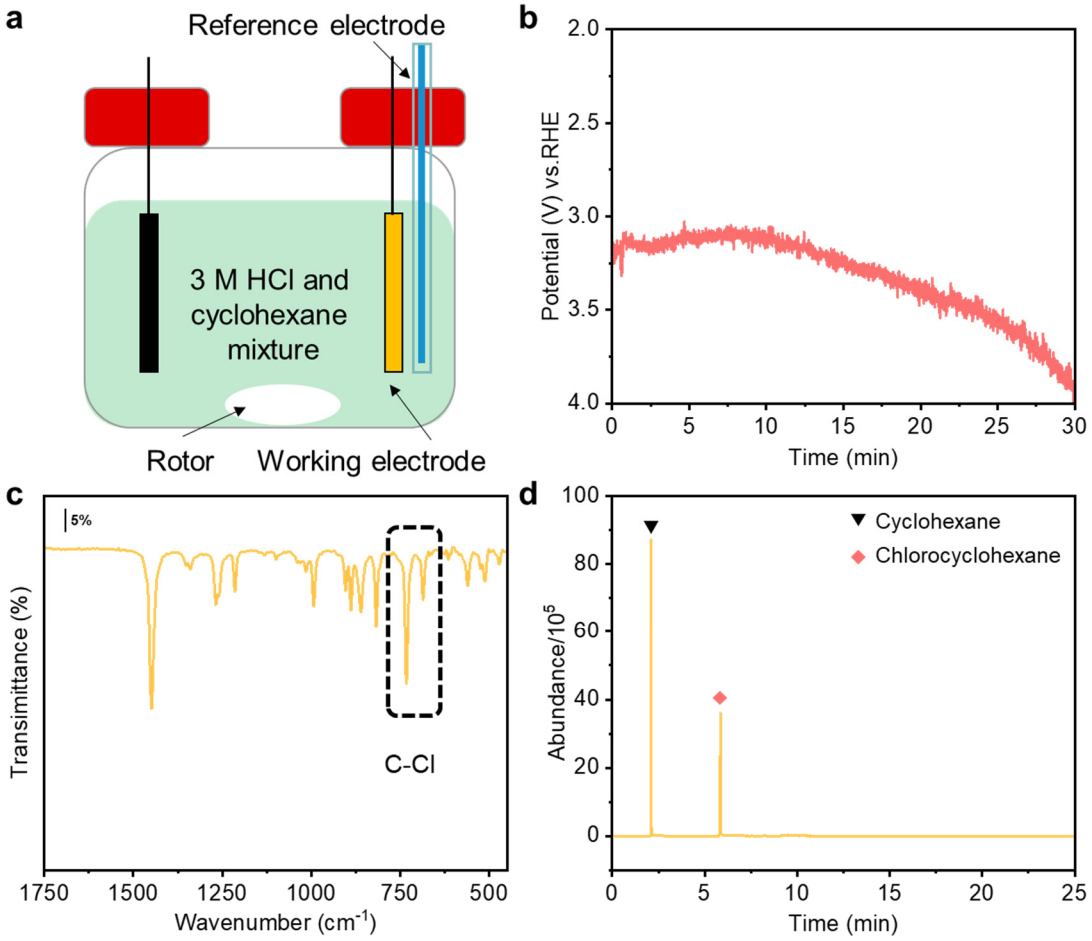

Fig. S48. (a) Schematic illustration of chlorocyclohexane production in the one cell configuration. (b) Applied potential as a function of time when a current of 5 A was applied using Pt/IrO_x as the catalyst. (c) FTIR spectroscopy of samples obtained with a current of 5 A using Pt/IrO_x as the catalyst. (d) GCMS results of samples obtained with a current of 5 A using Pt/IrO_x as the catalyst.

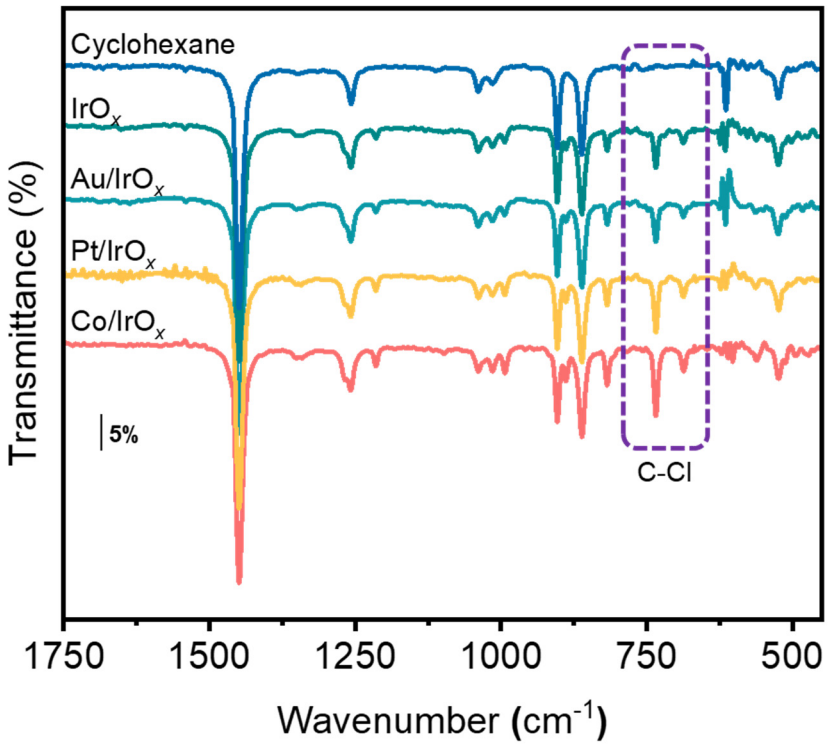

Fig. S49. FTIR spectroscopy of samples obtained using different electrocatalysts in 1.0 M KCl electrolyte at a current of 600 mA.

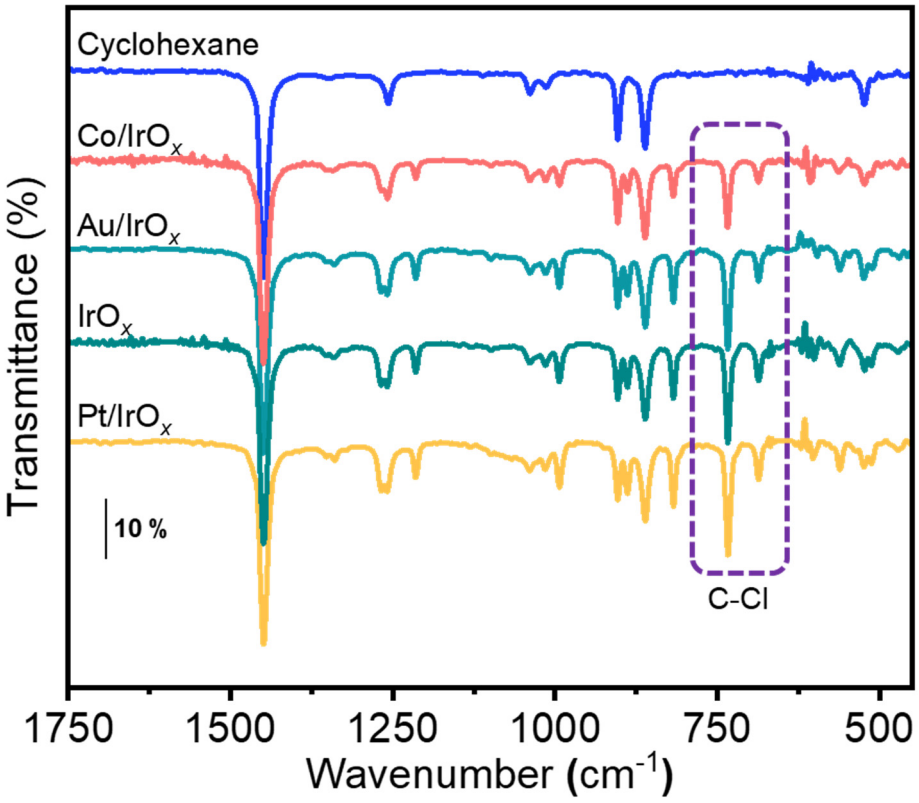

Fig. S50. FTIR spectroscopy of samples obtained using different electrocatalysts in 1.0 M KCl electrolyte at a current of 800 mA.

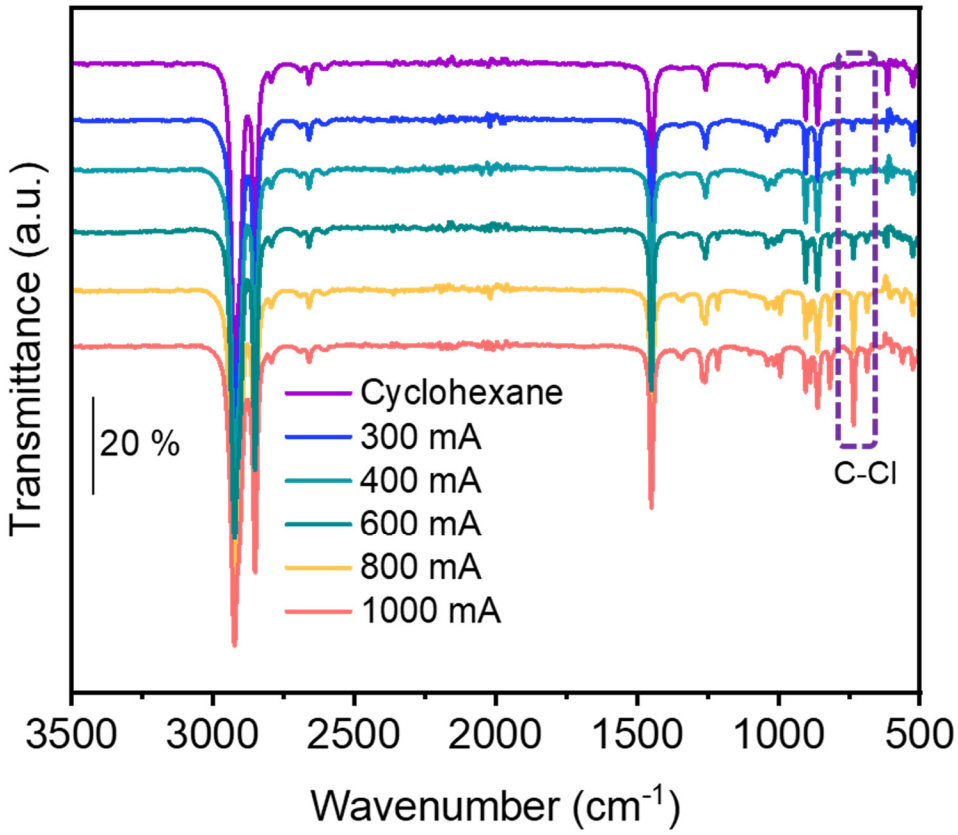

Fig. S51. FTIR spectroscopy of samples obtained using IrO_x in 1.0 M KCl electrolyte at various applied currents.

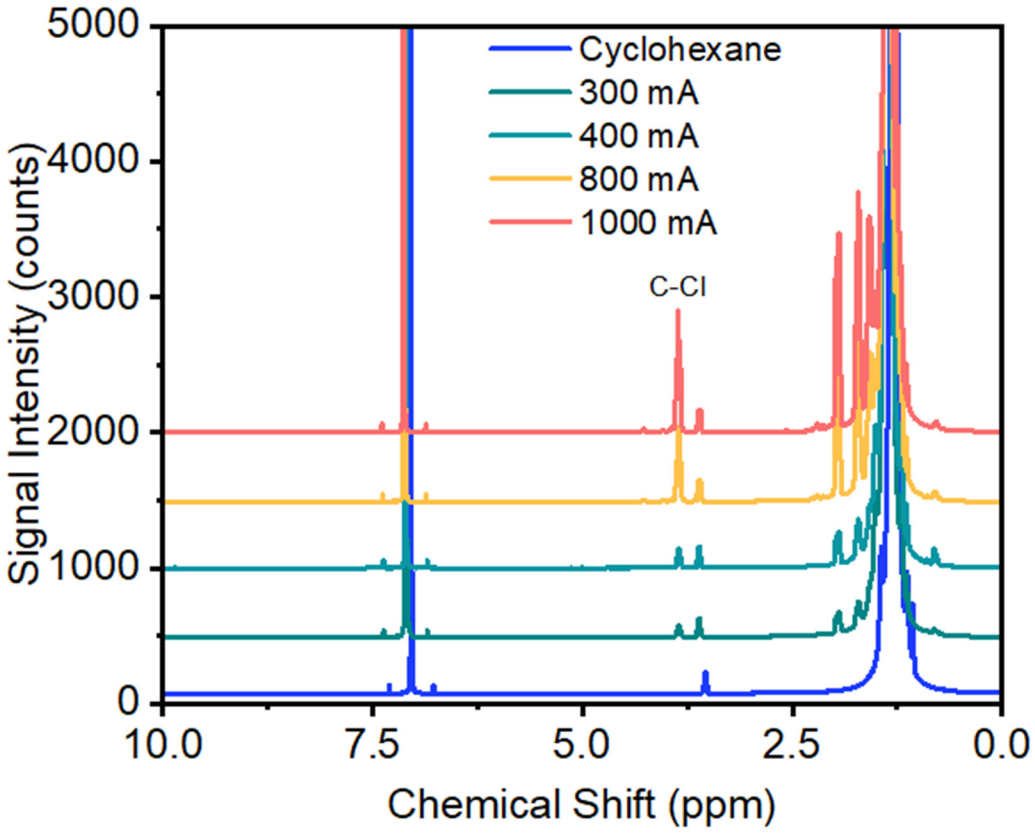

Fig. S52. ^{1}H-NMR spectroscopy of samples obtained by Pt/IrO_x in 1.0 M KCl electrolyte at various applied currents.

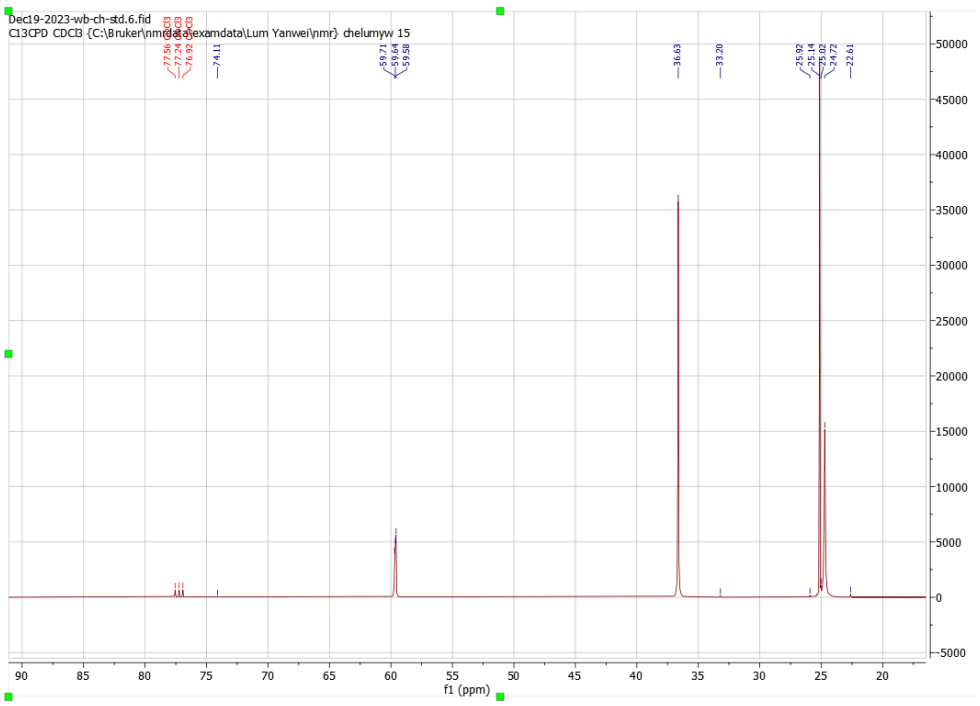

Fig. S53. Screenshot of the ^{13}C NMR spectra of standard chlorocyclohexane.

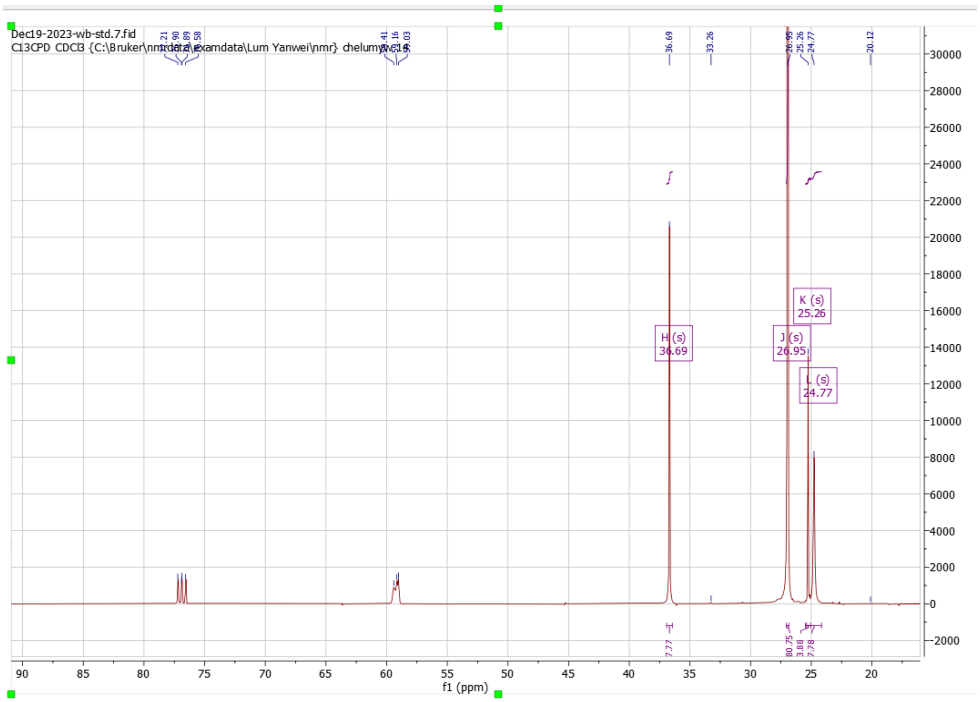

Fig. S54. Screenshot of the ^{13}C NMR spectra for the sample obtained with Pt/IrO_x at a current of 1000 mA with 5 ml cyclohexane added as the reactant.

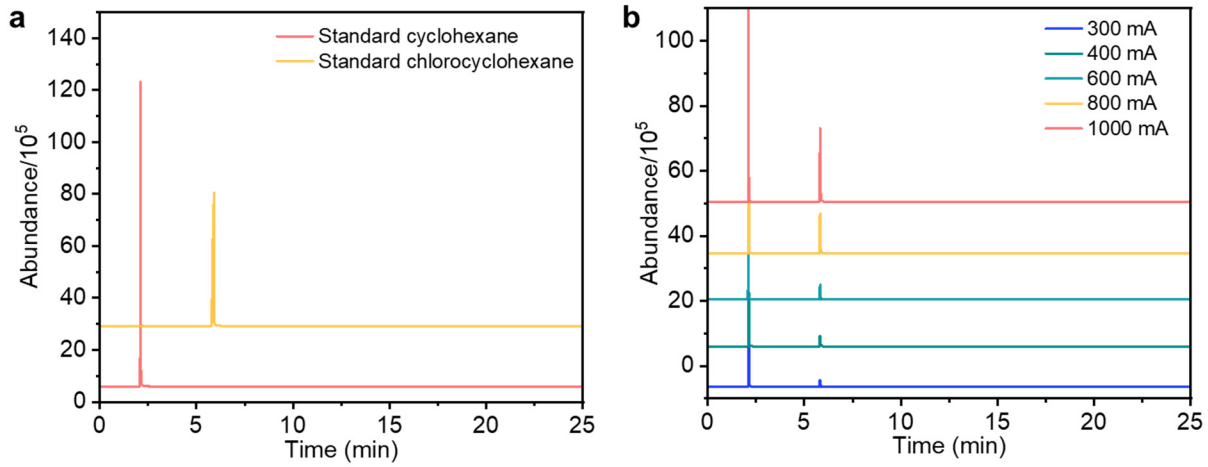

Fig. S55. (a) GCMS results of cyclohexane and chlorocyclohexane standard samples (b) Full GCMS results of samples in 1.0 M KCl electrolyte at various applied currents for Pt/IrO_x.

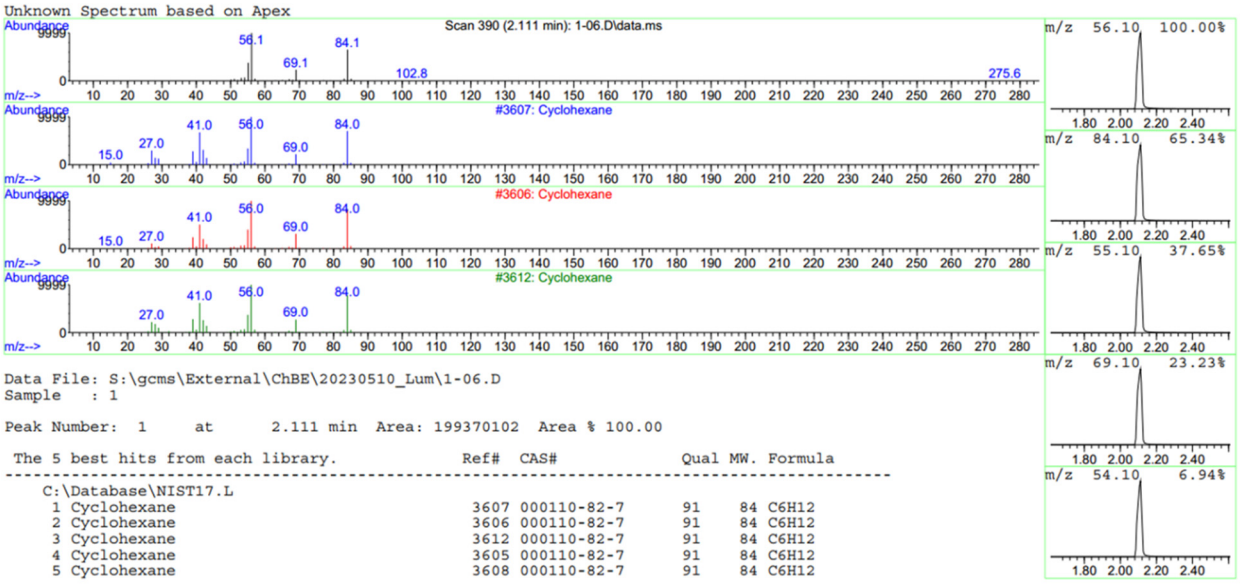

Fig. S56. MS spectrum of standard cyclohexane. Note: the mass range for testing was set from m/z 50-500.

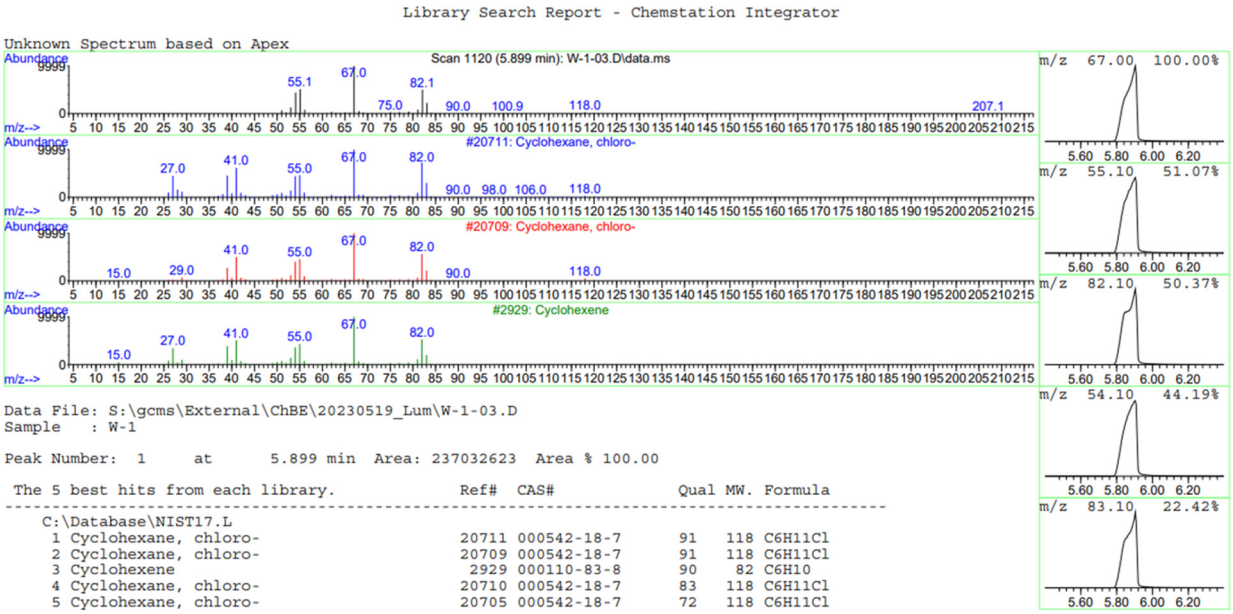

Fig. S57. MS spectrum of standard chlorocyclohexane. Note: the mass range for testing was set from m/z 50-500.

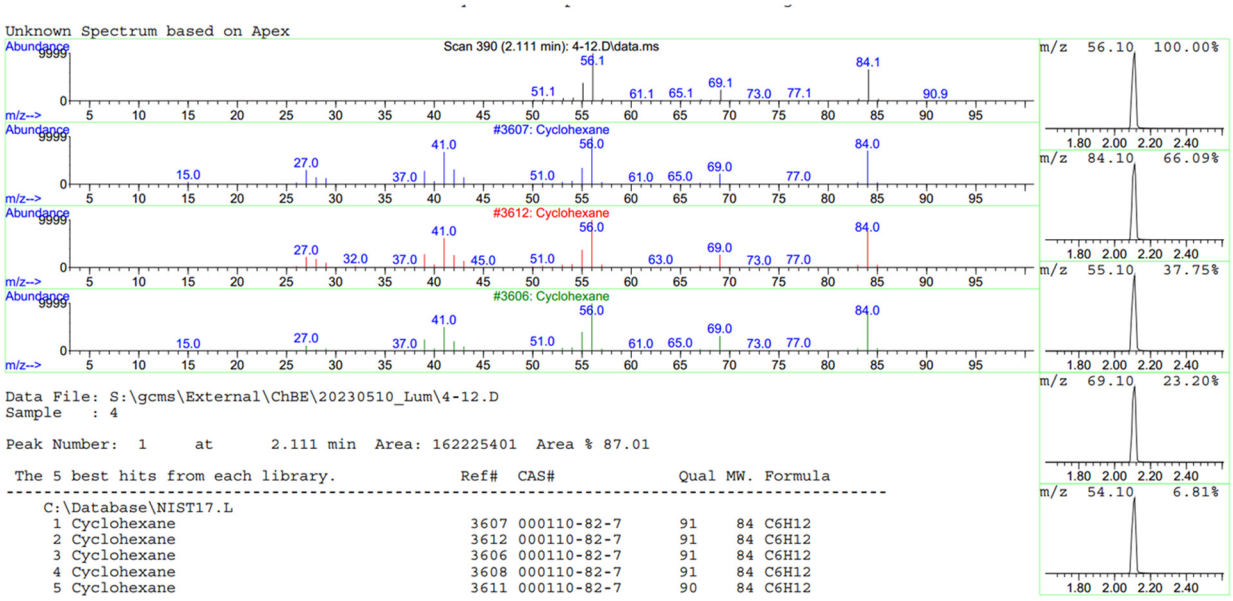

Fig. S58. MS spectrum of our sample from the GCMS peak at around 2.5 min. Note: the mass range for testing was set from m/z 50-500.

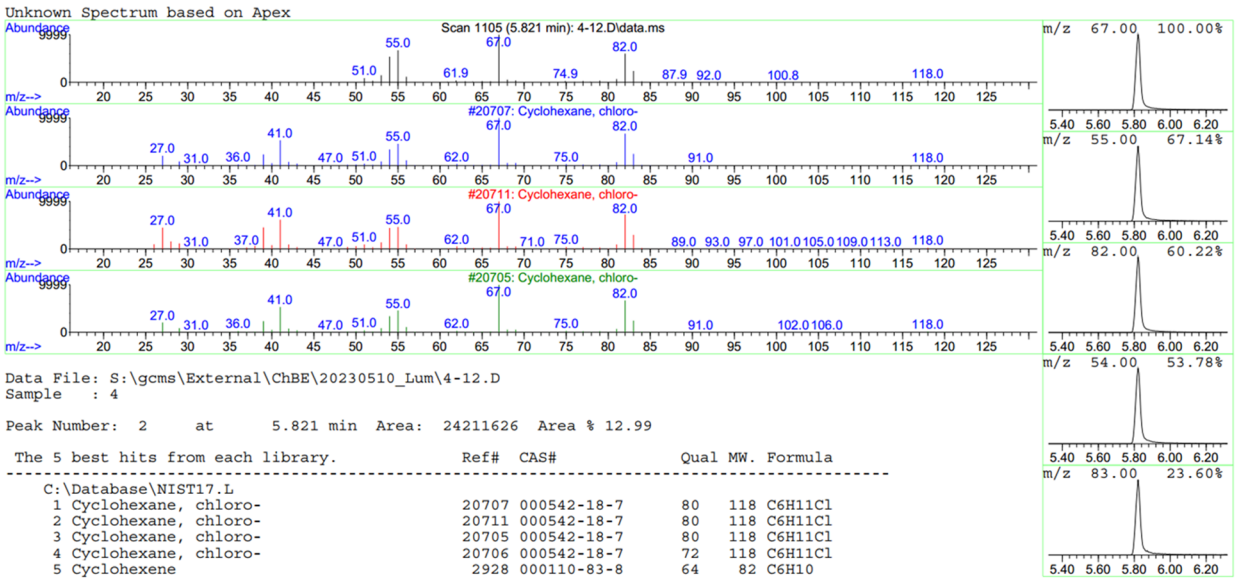

Fig. S59. MS spectrum of our sample from the GC peak at around 5.9 min. Note: the mass range for testing was set from m/z 50-500.

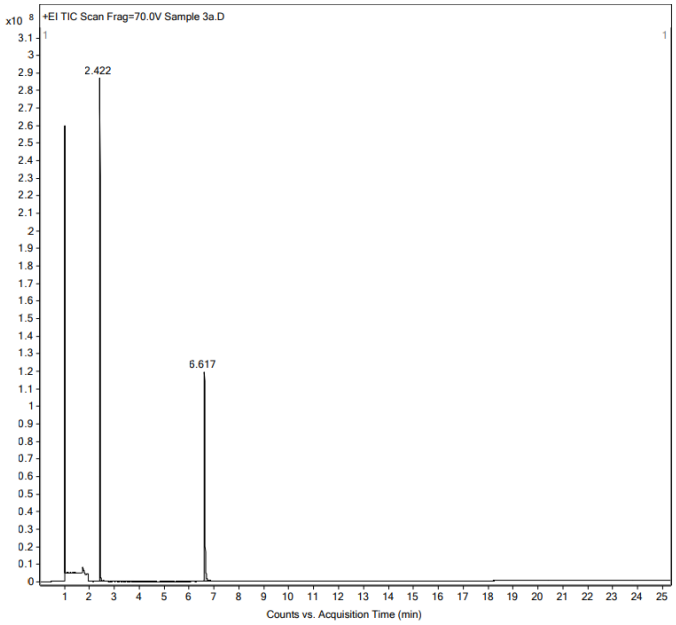

Fig. S60. Screenshot of the HR-GCMS data of our sample obtained at a current of 1000 mA using Pt/IrO_x as the electrode. 5 ml cyclohexane mixed with 45 ml 1 M KCl was used as the electrolyte, with a rotation speed of 500 rpm. The peak obtained at ~1 min belongs to the reference compound (perfluorotributylamine, PFTBA), which was used for accurate mass analysis.

Mass Spectrum SmartFormula Report

Sample Name	Sample 3	**Data File**	D:\04_External\ChBE\20231222\Sample 3a.D
Instrument Name	Agilent 7200 GC-QTOF	**IRM Calibration Status**	Success
Acq Method	EIHR_CalValve.ei_ChBE_Lum Yanwei_Wu Bo.M	**Acquired Time**	22/12/2023 4:35:50 PM (UTC+08:00)
Comment	ChBE, A/PLum Yanwei	**Operator**	WLK

Meas. m/z	**#**	**Formula**	**Calc. Mass**	**Err [ppm]**
84.0932	1	C6 H12	84.0934	2.38

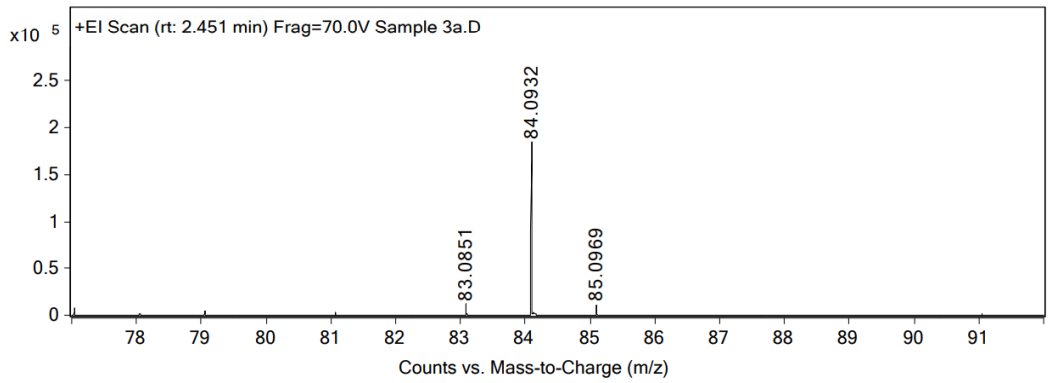

Fig. S61. Screenshot of the HR-MS spectrum belonging to the cyclohexane peak (2.4 min).

Mass Spectrum SmartFormula Report

Sample Name	Sample 3	**Data File**	D:\04_External\ChBE\20231222\Sample 3a.D
Instrument Name	Agilent 7200 GC-QTOF	**IRM Calibration Status**	Success
Acq Method	EIHR_CalValve.ei_ChBE_Lum Yanwei_Wu Bo.M	**Acquired Time**	22/12/2023 4:35:50 PM (UTC+08:00)
Comment	ChBE, A/PLum Yanwei	**Operator**	WLK

Meas. m/z	**#**	**Formula**	**Calc. Mass**	**Err [ppm]**
118.0546	1	C6 H11 Cl	118.0544	1.69

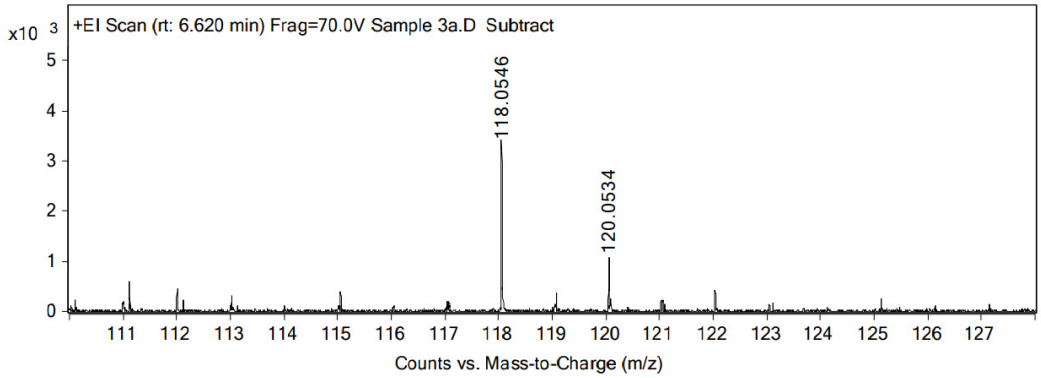

Fig. S62. Screenshot of the HR-MS spectrum belonging to the chlorocyclohexane peak (6.6 min).

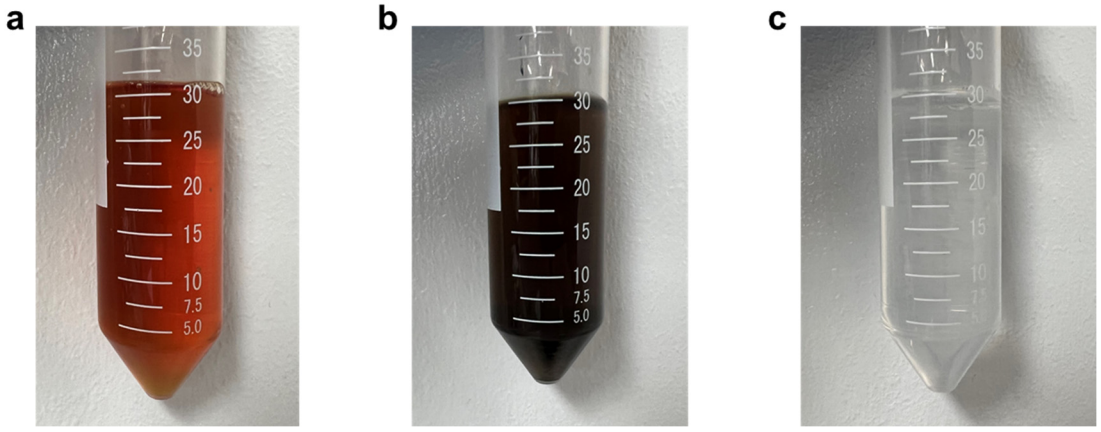

Fig. S63. (a) Digital photograph of the anolyte after addition of excess 10% KI solution. A brown coloration is observed due to oxidation of I^- to form I_2. (b) Digital photograph of the same anolyte after starch solution was added, forming a dark blue starch-iodine complex. (c) Digital photograph of the anolyte after titration with $Na_2S_2O_3$, yielding a clear colourless solution.

The equation of the reaction for I_2 and $S_2O_3^{2-}$ is listed below:

$$2S_2O_3^{2-} + I_2 \rightarrow S_4O_6^{2-} + 2I^-$$

Table S5. Collated FE towards unreacted chlorine/hypochlorite species at various applied currents density for the IrO_x anode.

Current	Amount of $Na_2S_2O_3$ added (mmol)	Amount of unreacted chlorine/hypochlorite species	FE loss due to the unreacted hypochlorite (%)
300	3.0	1.5	53.4%
400	3.6	1.8	47.1%
600	4.6	2.3	41.9%
800	2.8	1.4	18.7%
1000	1.6	0.8	8.3%

Table S6. Collated FE towards unreacted chlorine/hypochlorite species at various applied currents density for the Co/IrO_x anode.

Current	Amount of $Na_2S_2O_3$ added (mmol)	Amount of unreacted chlorine/hypochlorite species	FE loss due to the unreacted hypochlorite (%)
300	3.6	1.8	64.2%
400	2.4	1.2	30.9%
600	2.0	1.0	17.1%
800	3.4	1.7	22.4%
1000	5.6	2.8	28.3%

Table S7. Collated FE towards unreacted chlorine/hypochlorite species at various applied currents density for the Au/IrO_x anode.

Current	Amount of $Na_2S_2O_3$ added (mmol)	Amount of unreacted chlorine/hypochlorite species	FE loss due to the unreacted hypochlorite (%)
300	4.4	2.2	76.1%
400	4.2	2.1	56.3%
600	6.0	3.0	53.7%
800	5.6	2.8	37.2%
1000	4.4	2.2	21.8%

Table S8. Collated FE towards unreacted chlorine/hypochlorite species at various applied currents density for the Pt/IrO_x anode.

Current	Amount of $Na_2S_2O_3$ added (mmol)	Amount of unreacted chlorine/hypochlorite species	FE loss due to the unreacted hypochlorite (%)
300	2.6	1.3	45.8%
400	3.2	1.6	42.3%
600	3.8	1.9	33.8%
800	1.6	0.8	10.3%
1000	0.8	0.4	3.6%

Fig. S64. Digital photograph of the product obtained after 100 h of operation, consisting of a mixture of cyclohexane and chlorocyclohexane. Note: the aqueous electrolyte was removed using a separating funnel. The 100 h measurement was separated into 25 cycles, with 4 h in each cycle. Every cycle uses 90 ml of 1 M KCl electrolyte and 10 ml of cyclohexane.

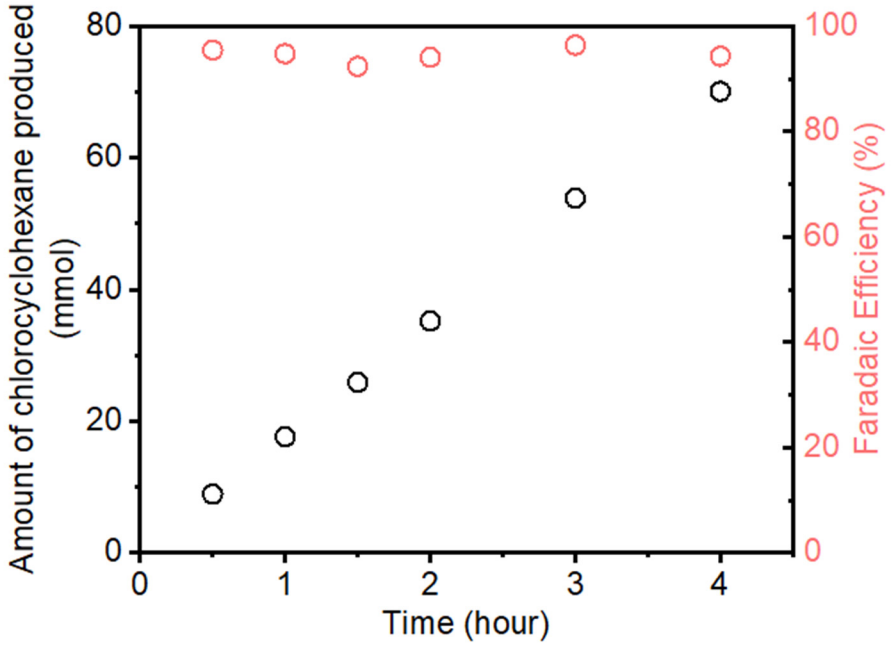

Fig. S65. Amount of chlorocyclohexane produced and the corresponding FE value during a 4 h period testing for Pt/IrO_x at a current of 1 A.

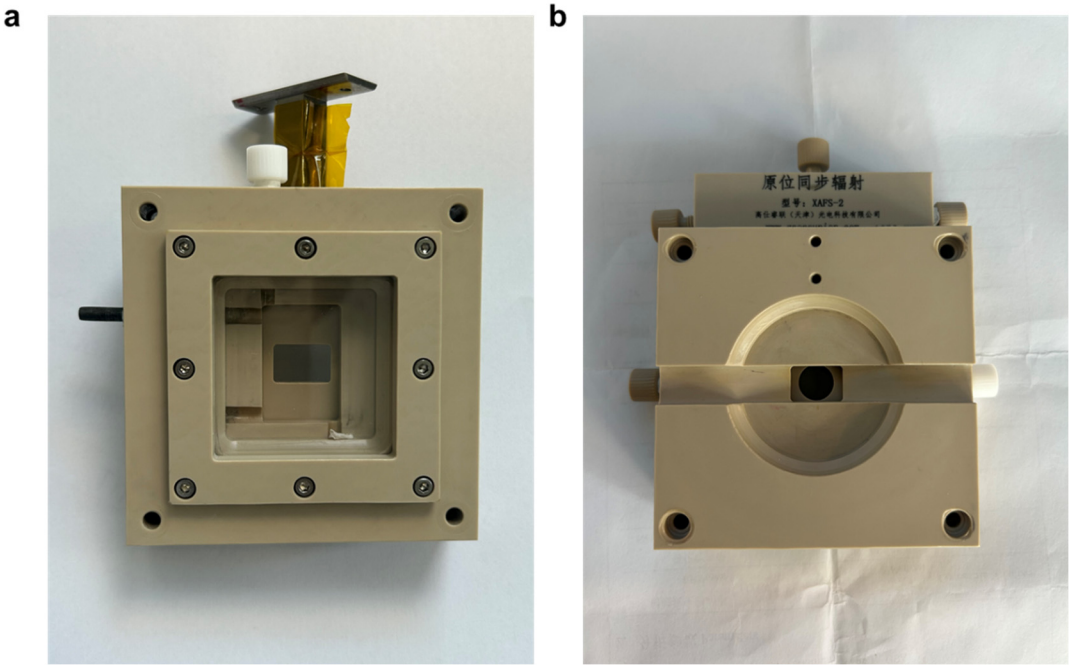

Fig. S66. Digital photograph of cell used for *in-situ* XAS measurements (front view) under (a) fluorescence mode and (b) transmission mode.

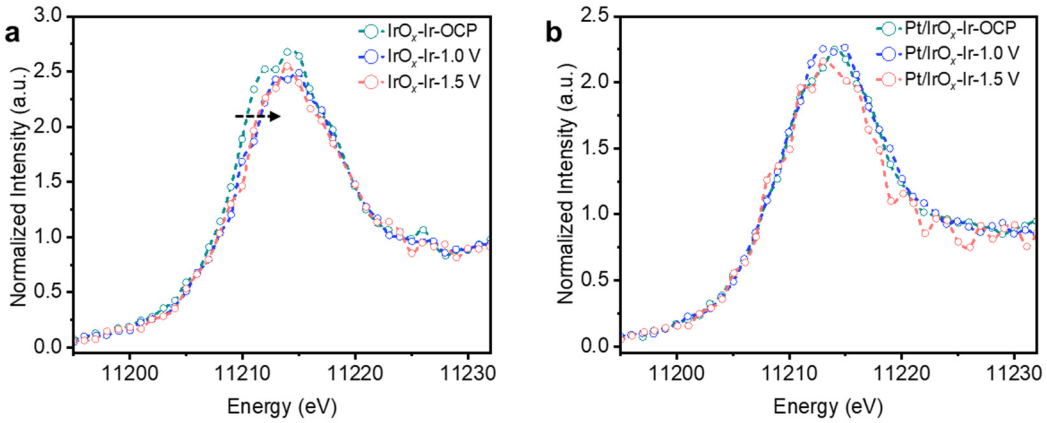

Fig. S67. Operando Ir L_3-edge XANES spectra of (c) IrO_x and (d) Pt/IrO_x collected at OCP, 1 V and 1.5 V vs. Ag/AgCl in 1 M KCl electrolyte. Standard IrO_2 sample is included as a reference.

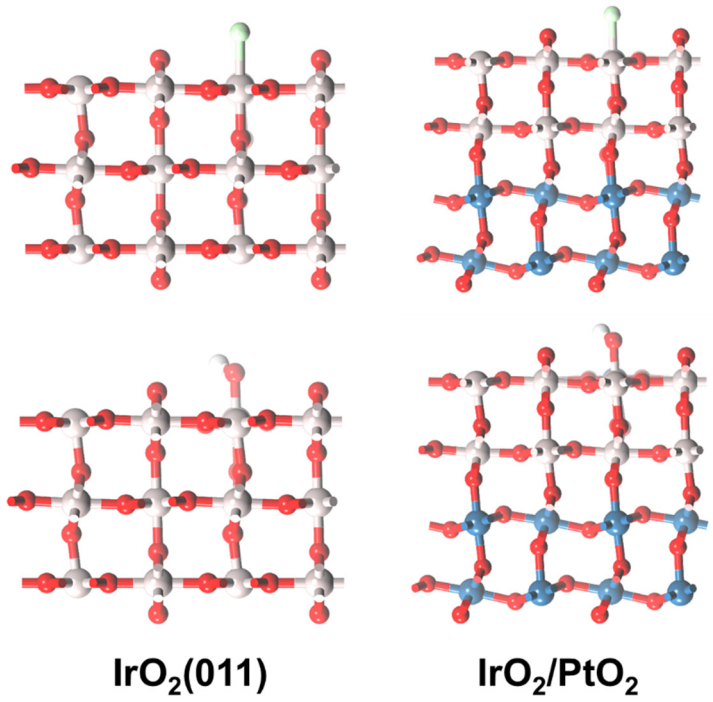

Fig. S68. Side views of $IrO_2(011)$, IrO_2/PtO_2, PtO_2/IrO_2 with adsorbed *Cl and *OH. The white, red, green, gray and blue spheres represent H, O, Cl, Ir and Pt atoms respectively.

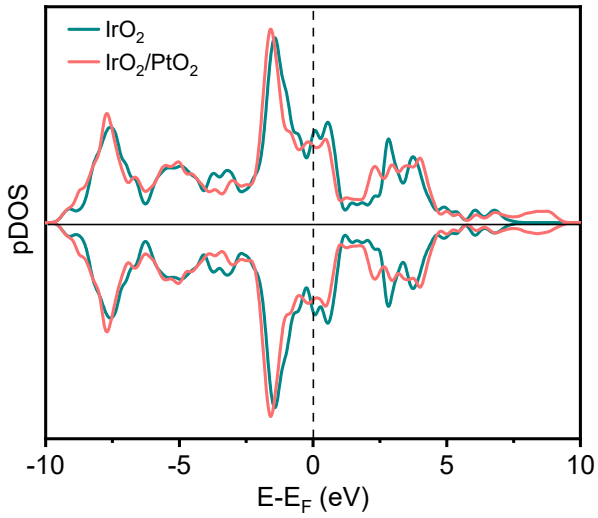

Fig. S69. Projected density of states (pDOS) diagrams of Ir in IrO_2 and IrO_2/PtO_2.

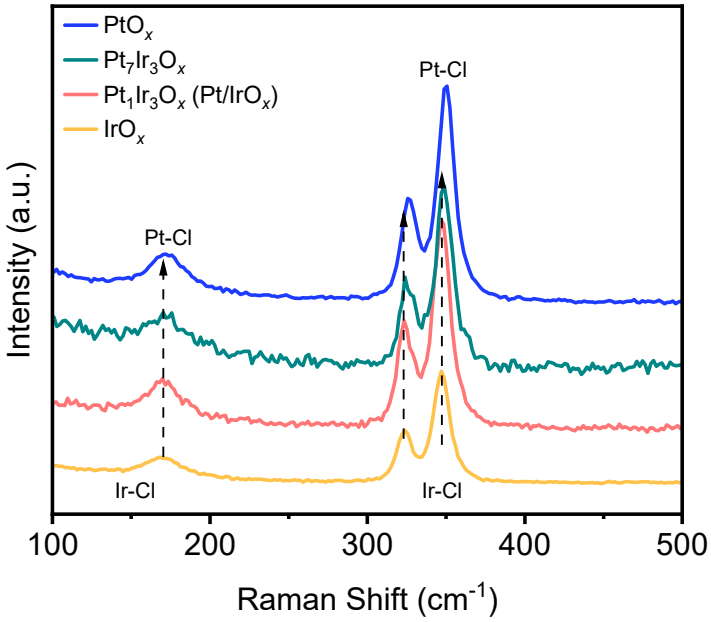

Fig. S70. The Raman spectra of different signal obtained by different catalysts under a potential of 1.2 V vs. Ag/AgCl using 1 M KCl as the electrolyte.

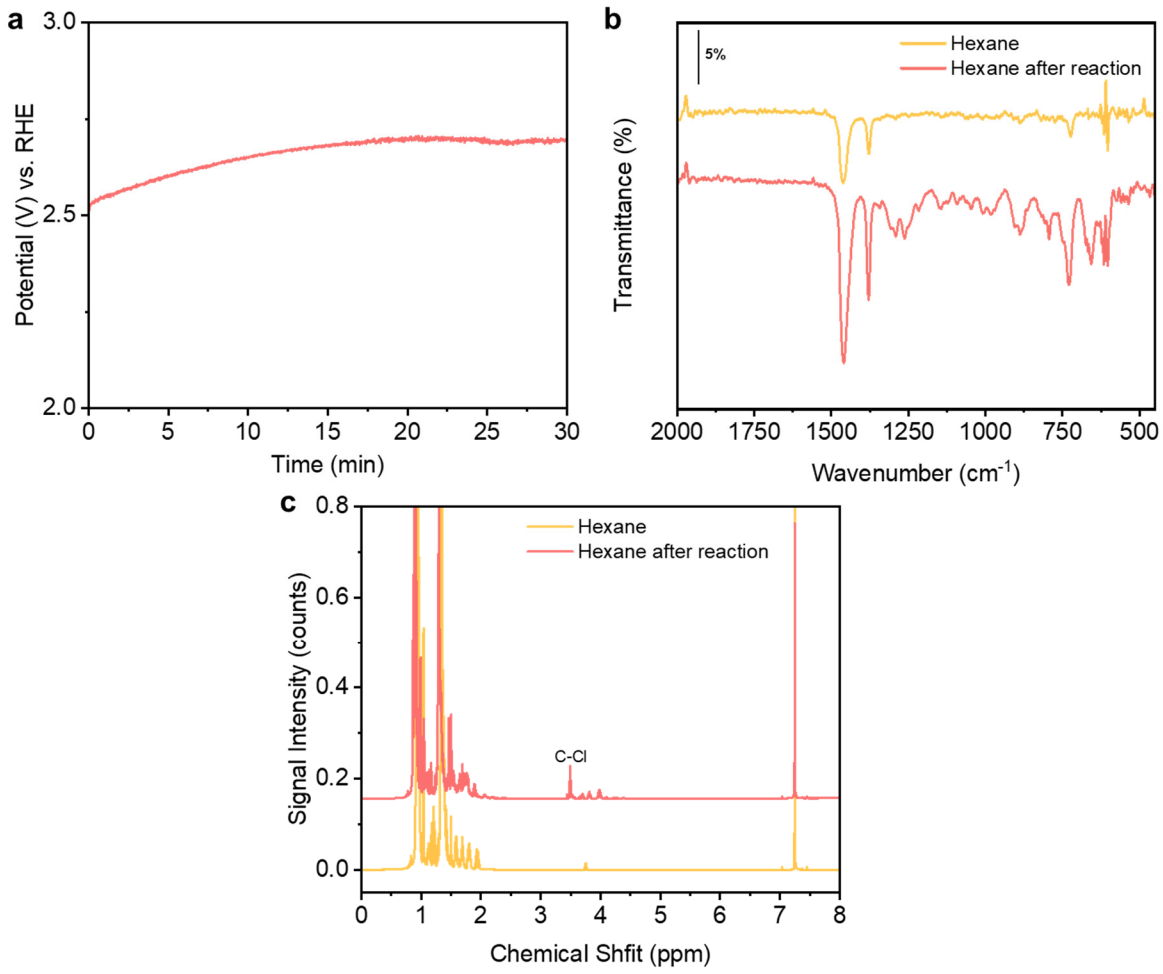

Fig. S71. (a) Applied potential as a function of time with an applied current of 800 mA for hexane halogenation using IrO_x as the anode. (b) FTIR spectroscopy of the sample after reaction and standard hexane. (c) ^{1}H-NMR spectroscopy of sample after reaction and standard hexane.

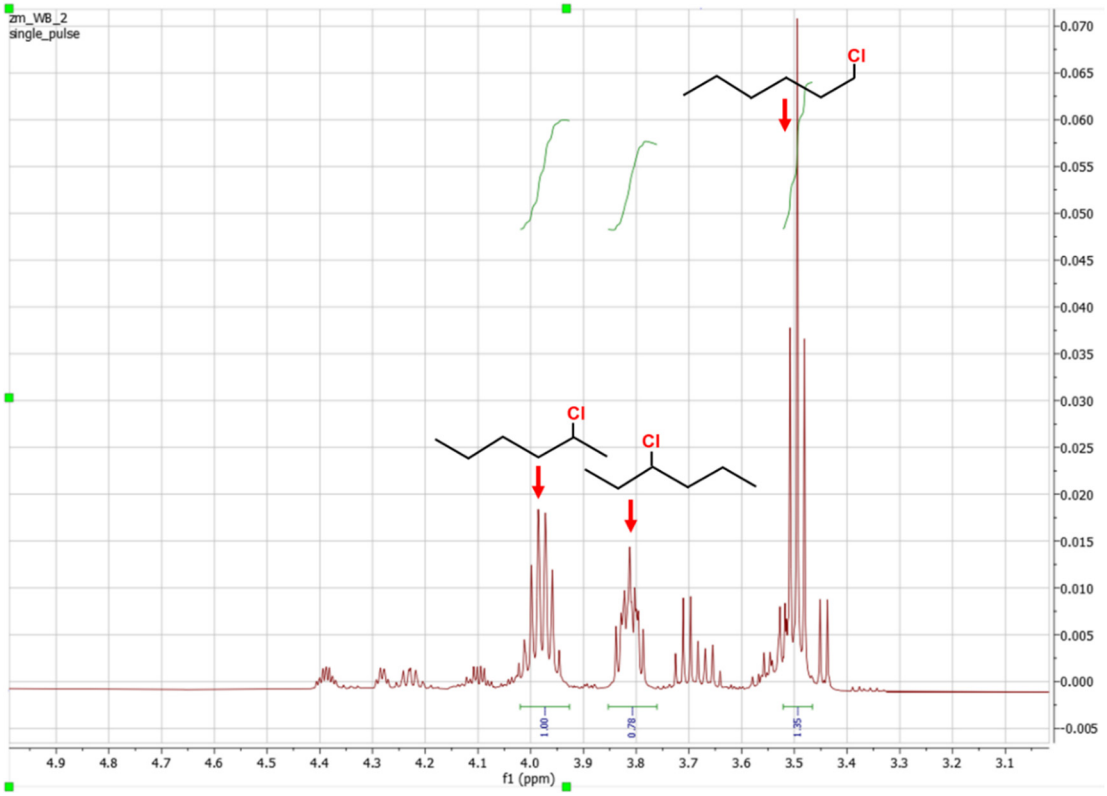

Fig. S72. Screenshot of the ^{1}H-NMR results for our sample obtained at a current of 1000 mA using IrO_x as the catalyst for the chlorination of hexane. Each peak is labelled according to the assigned product and integration areas for each case are also displayed. For hexane, the ratios of the 1-chlorohexane, 2-chlorohexane and 3-chlorohexane products generated are 0.675:0.78:1 respectively, based on the integration areas of ^{1}H NMR spectra of collected sample. The corresponding product specificity for 1-chlorohexane, 2-chlorohexane and 3-chlorohexane products are 15.9%, 36.8%, and 47.2%. With 10.8% of hexane converted for a short 30 min test, the corresponding yield for 1-chlorohexane, 2-chlorohexane and 3-chlorohexane products are 1.7%, 3.97%, and 5.1%.

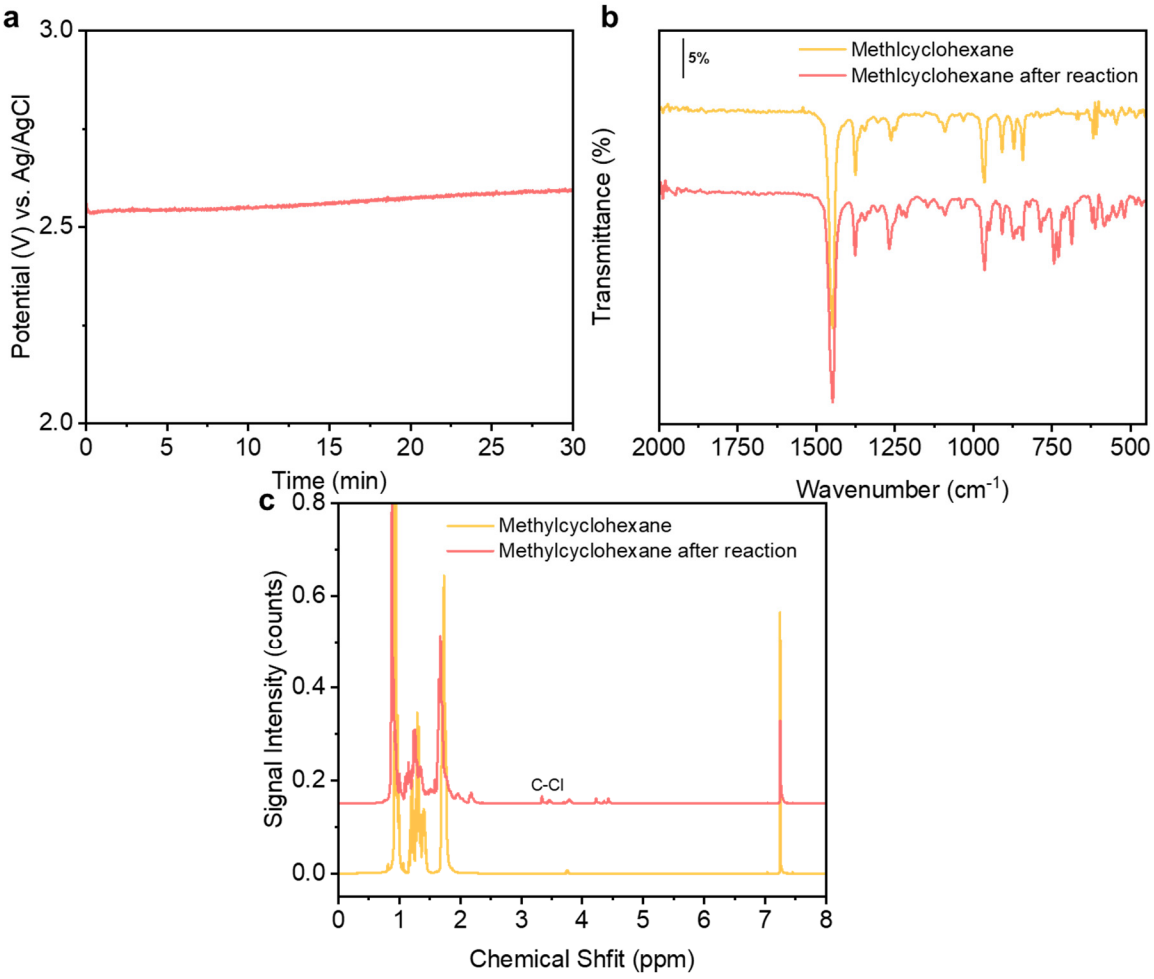

Fig. S73. (a) Applied potential as a function of time with an applied current of 800 mA for methylcyclohexane halogenation using IrO_x as the anode. (b) FTIR spectroscopy of the sample after reaction and standard methylcyclohexane. (c) ^{1}H-NMR spectroscopy of sample after reaction and standard hexane.

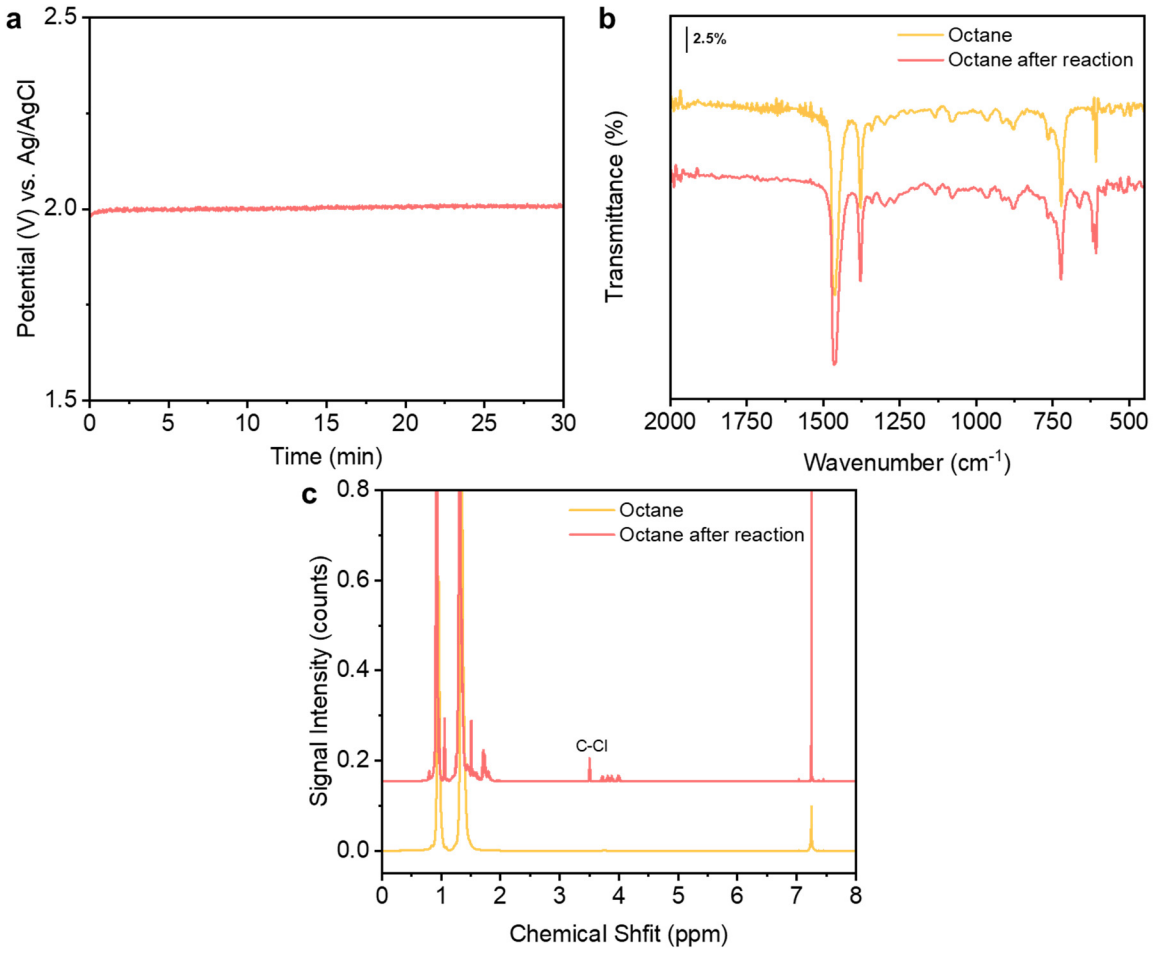

Fig. S74. (a) Applied potential as a function of time with an applied current of 800 mA for octane halogenation using IrO_x as the anode. (b) FTIR spectroscopy of the sample after reaction and standard octane. (c) ^{1}H-NMR spectroscopy of sample after reaction and standard octane. (d) Electrochemical C-H halogenation of octane to form chlorooctane.

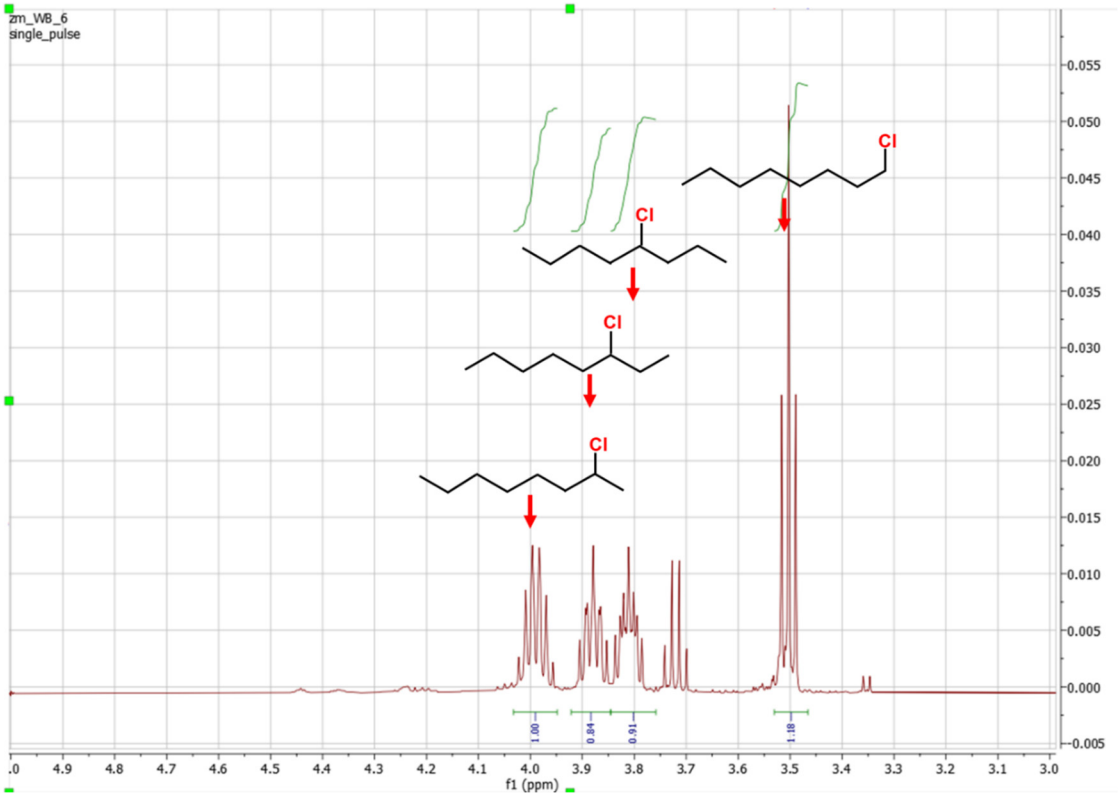

Fig. S75. Screenshot of the ^{1}H-NMR results for our sample obtained at a current of 1000 mA using IrO_x as the catalyst for the chlorination of octane. Each peak is labelled according to the assigned product and integration areas for each case are also displayed. The ratios of the 1-chloroctane, 2-chloroctane, 3-chloroctane and 4-chloroctane are 0.59:1:0.84:0.91 also obtained from the integration areas of ^{1}H NMR spectra of collected sample. The corresponding product selectivity for 1-chloroctane, 2-chloroctane, 3-chloroctane and 4-chloroctane are 9.7%, 32.8%, 27.5%, and 29.8%. During a 30 min testing, 11.6% of octane was converted. Therefore, the yield for 1-chloroctane, 2-chloroctane, 3-chloroctane and 4-chloroctane are 1.1%, 3.8%, 3.2%, and 3.5%.

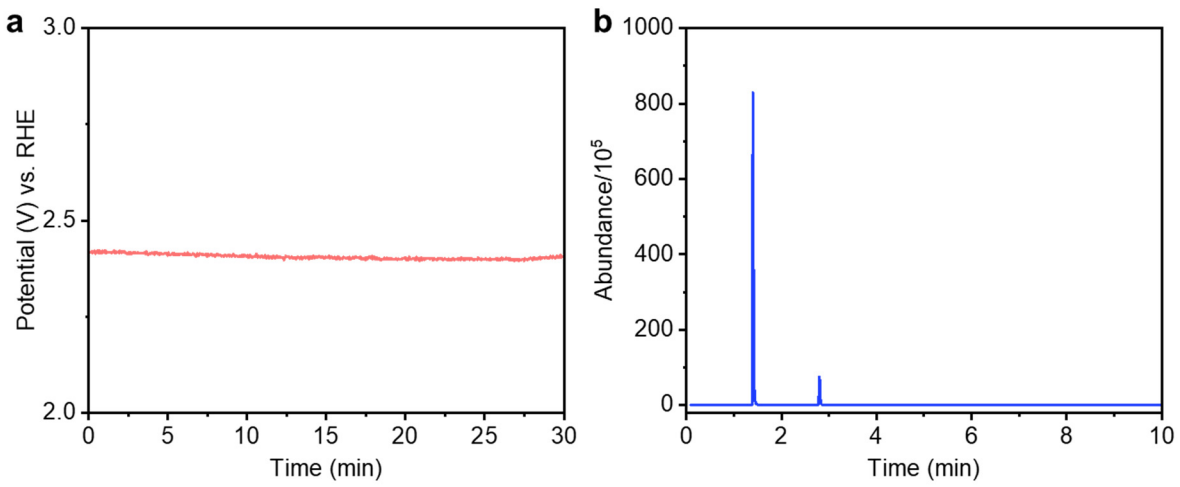

Fig. S76. (a) Applied potential as a function of time with an applied current of 1000 mA (200 mA/cm^2) for cyclopentane chlorination using Pt/IrO$_x$ as the anode. (b) GCMS analysis of samples obtained using KCl and cyclopentane mixture as the electrolyte under a current of 1000 mA with Pt/IrO$_x$ used as the anode for 30 min.

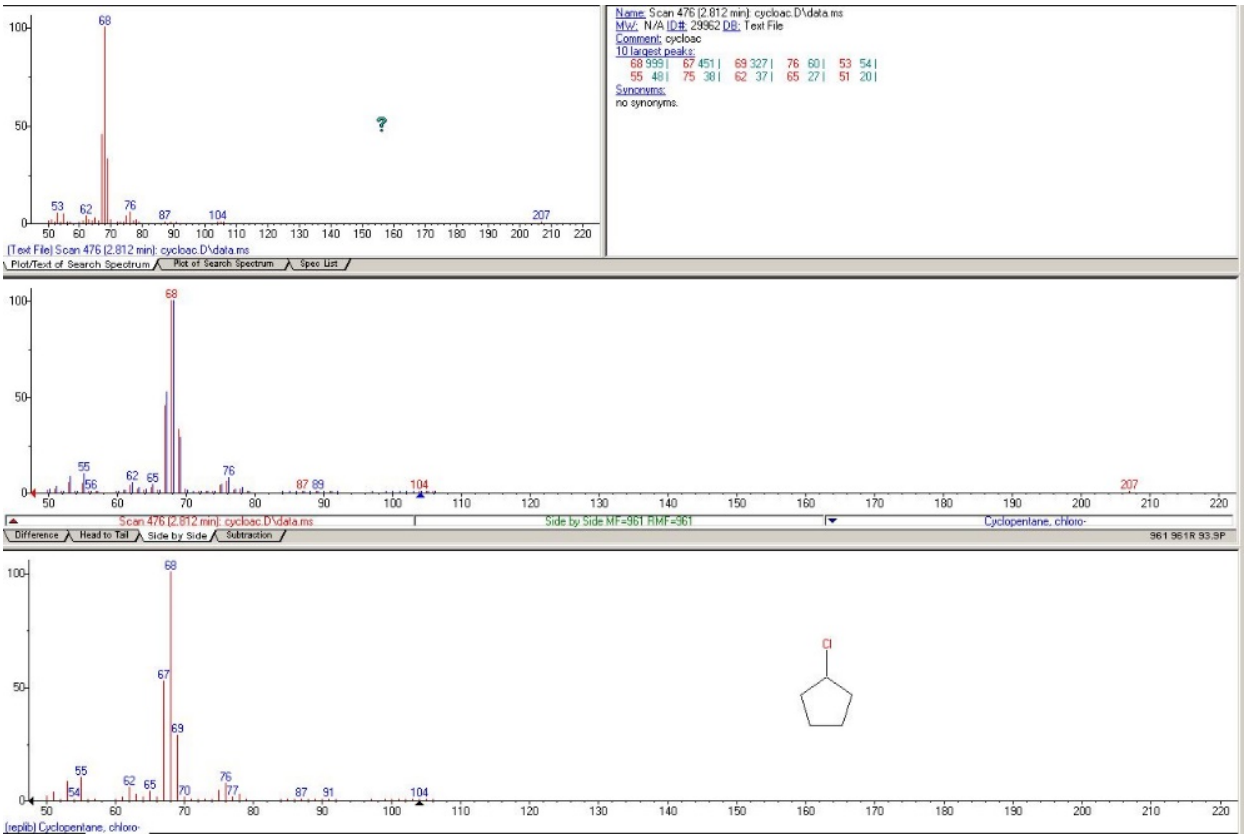

Fig. S77. MS spectrum of our sample from the GCMS peak at around 2.8 min.

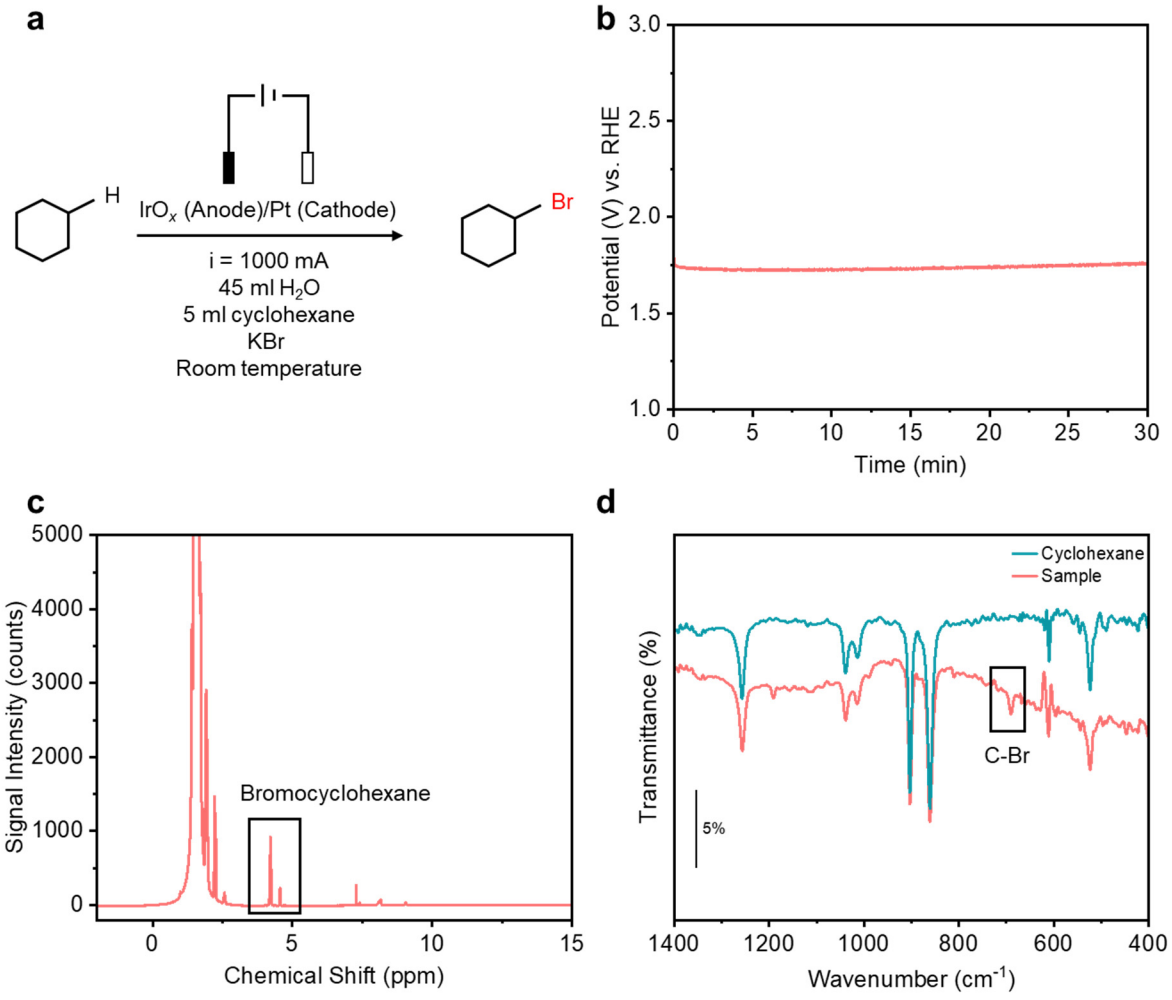

Fig. S78. (a) Conditions for bromocyclohexane production. (b) Applied potential as a function of time with an applied current of 1000 mA (200 mA/cm^2) for bromination of cyclohexane using IrO_x as the anode. (c) ^{1}H-NMR spectroscopy of the sample after reaction. (d) FTIR spectroscopy of the sample after reaction and a cyclohexane standard for comparison.

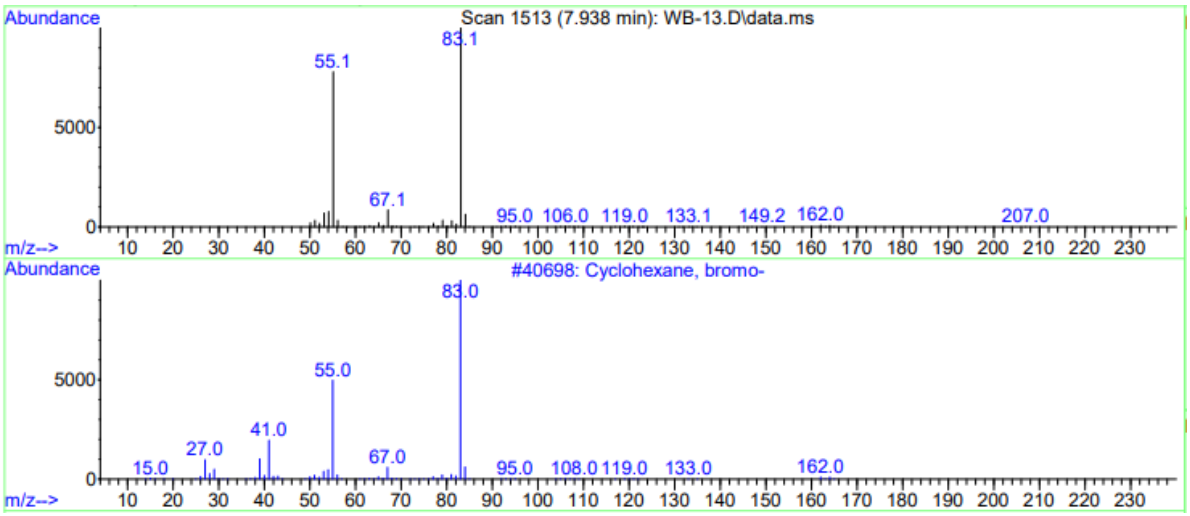

Fig. S79. Mass spectrum data of our sample for bromination of cyclohexane (top) and the NIST standard spectrum for comparison (bottom). Note: the mass range for testing was set from m/z 50-500.

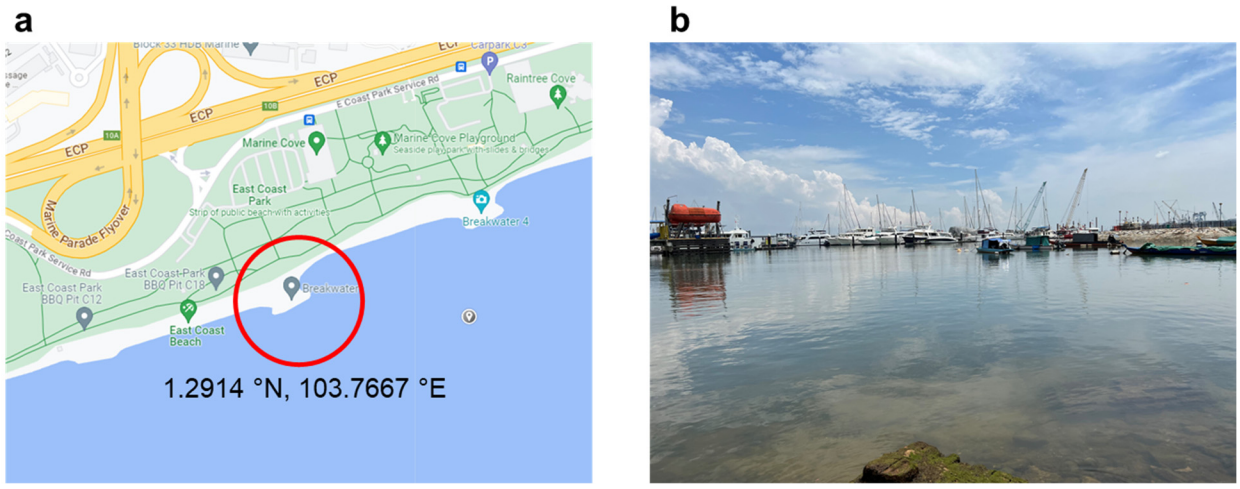

Fig. S80. (a) Position on Google maps and (b) picture of the location where the seawater used in this work was collected.

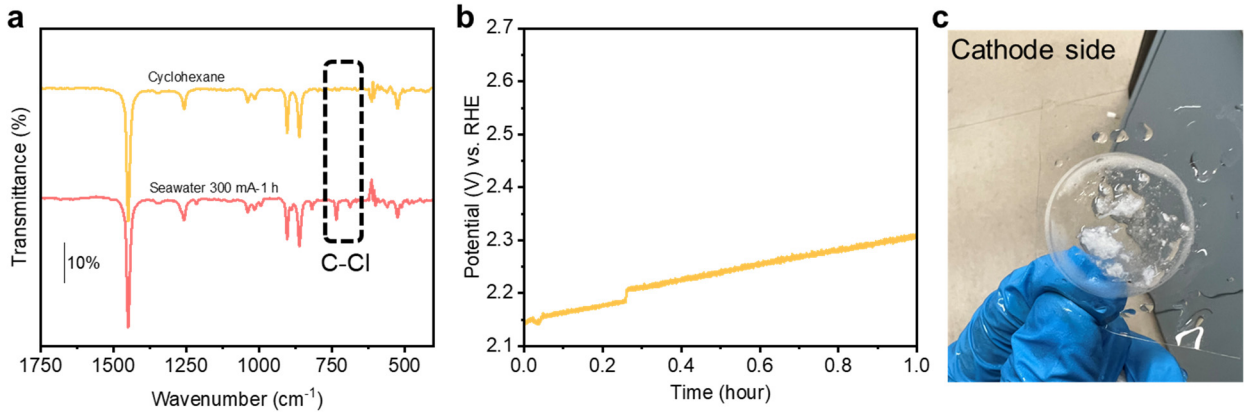

Fig. S81. (a) FTIR spectroscopy of sample with untreated seawater after an electrolysis time of 1 h at an applied current of 300 mA. (b) Applied potential as a function of time during the 1 h test at an applied current of 300 mA. (c) Digital photograph of membrane facing the cathode side, where a white precipitate is observed.

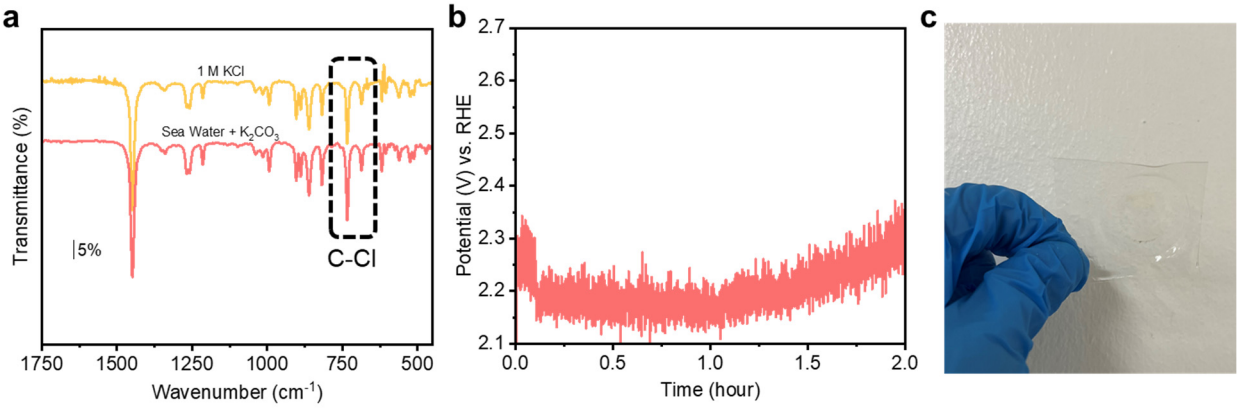

Fig. S82. (a) FTIR spectroscopy of sample with using treated seawater (K_2CO_3 was added to remove Ca^{2+} and Mg^{2+}) after an electrolysis time of 2 h at an applied current of 300 mA. (b) Applied potential as a function of time for the 2 h test at a current of 300 mA. (c) Digital photograph of the membrane on the cathode side.

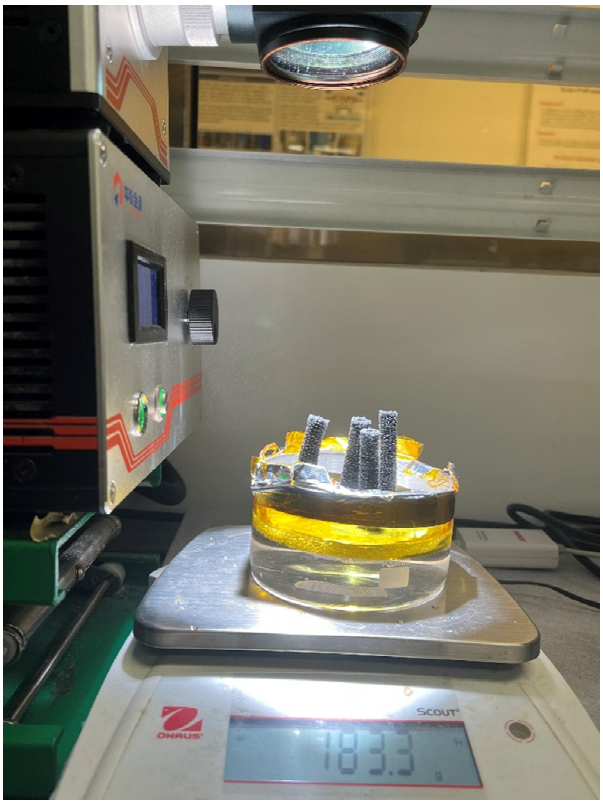

Fig. S83. Picture taken of the setup used for solar evaporation reverse osmosis.

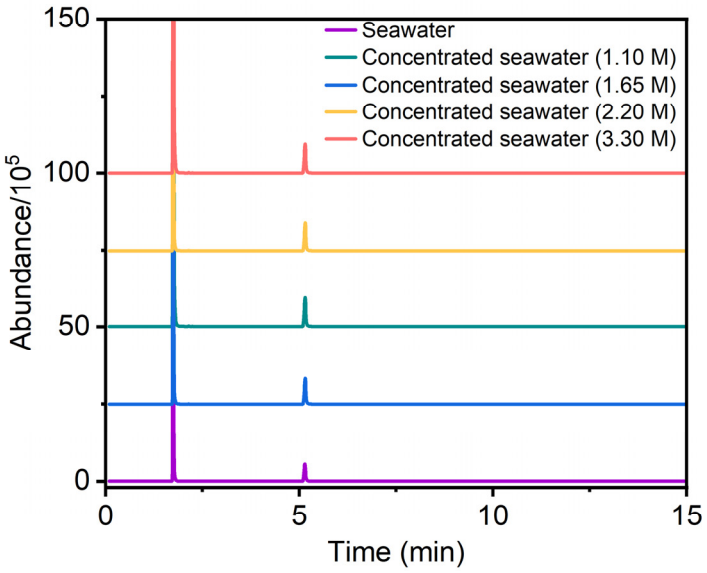

Fig. S84. GCMS analysis of samples obtained with different seawater (K_2CO_3 was added to remove Ca^{2+} and Mg^{2+}) as the electrolyte under a current of 1000 mA with Pt/IrO_x used as catalyst.

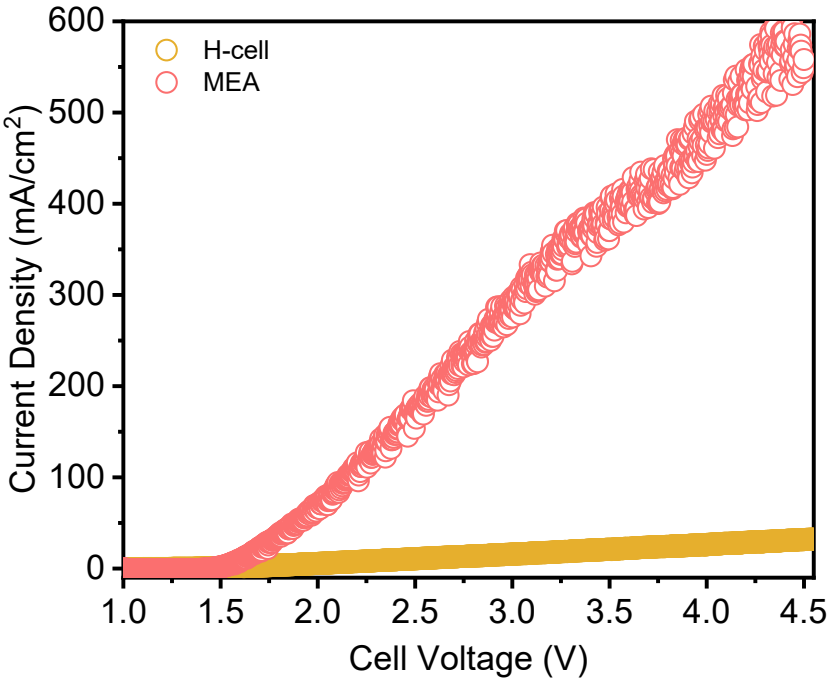

Fig. S85. Linear sweep voltammetry (LSV) curves of the H-cell and MEA cell in a two-electrode configuration in electrolyte consisting of 45 ml of 2 M HCl with 5ml of cyclohexane as the anolyte with 0.5 M H_2SO_4 as the catholyte.

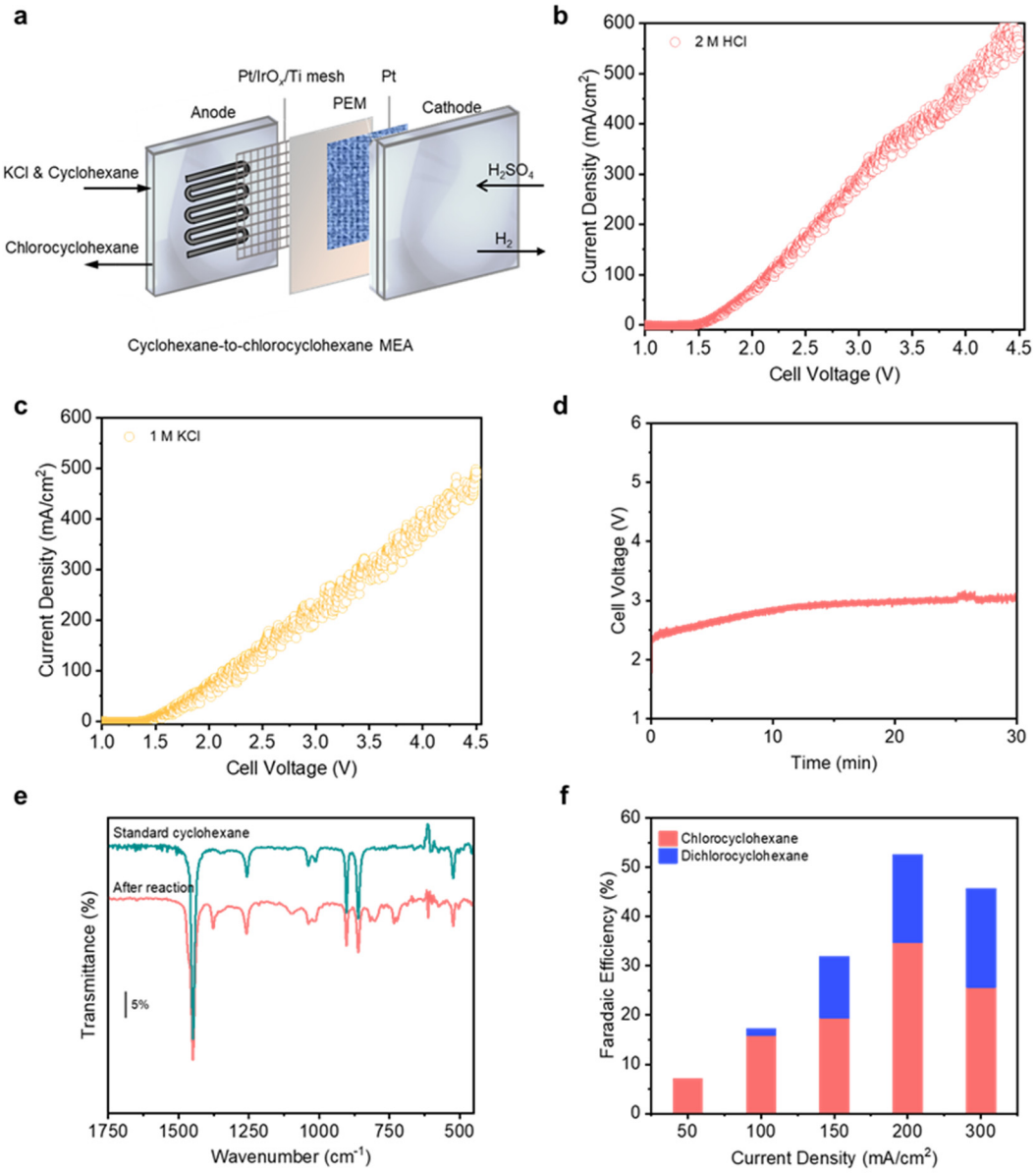

Fig. S86. (a) Schematic illustrating the setup used for the MEA cell. Current density as a function of total cell voltage using: (b) 2 M HCl, and (c) 1 M KCl as the electrolyte. (d) The FTIR spectroscopy of samples obtained by using 2 M HCl and cyclohexane mixture as the reactant with a current density of 200 mA/cm^2. (e) The cell voltage of the whole system under a current density of 200 mA/cm^2 with a test duration of 30 min using HCl and cyclohexane mixture as the reactant. (f) FE to chlorocyclohexane and dichlorocyclohexane at different current densities using the MEA based cell with 2 M HCl electrolyte and cyclohexane as the reactant.

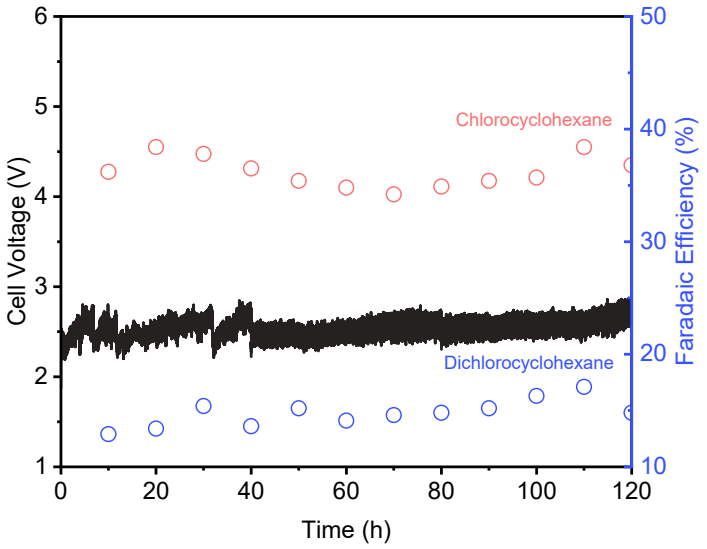

Fig. S87. Product FE and cell voltage during the extended 120 h testing period using the MEA system at a current density of 200 mA/cm^2 with 1500 ml of 2 M HCl and 100 ml cyclohexane mixture as the electrolyte.

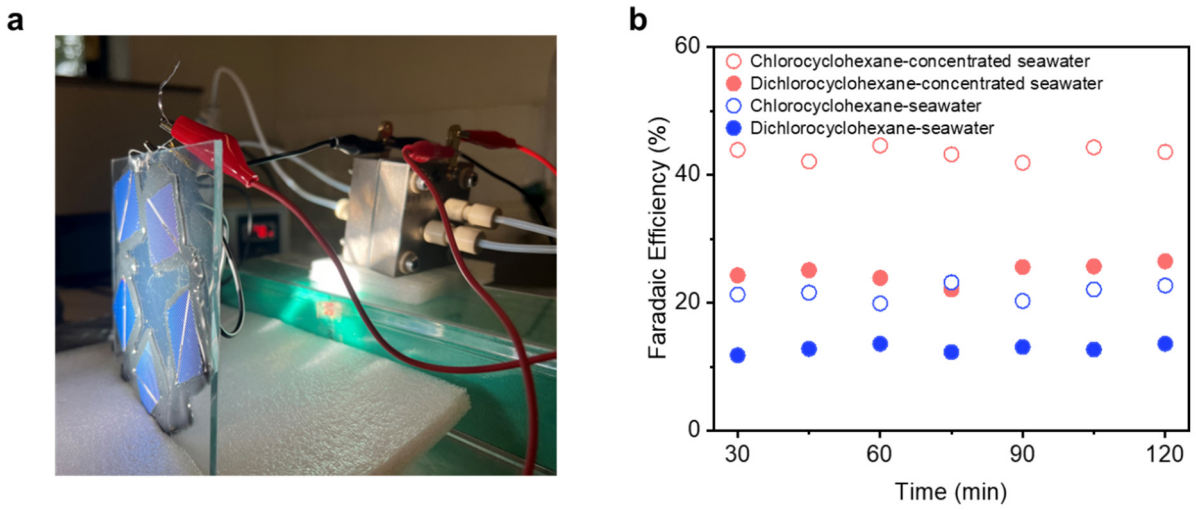

Fig. S88. (a) Picture taken of the solar-driven system for chlorination of cyclohexane with the MEA cell using seawater as the electrolyte. (b) Product FE obtained during 120 min of electrolysis powered by 1-sun solar illumination with seawater or concentrated seawater as the electrolyte.

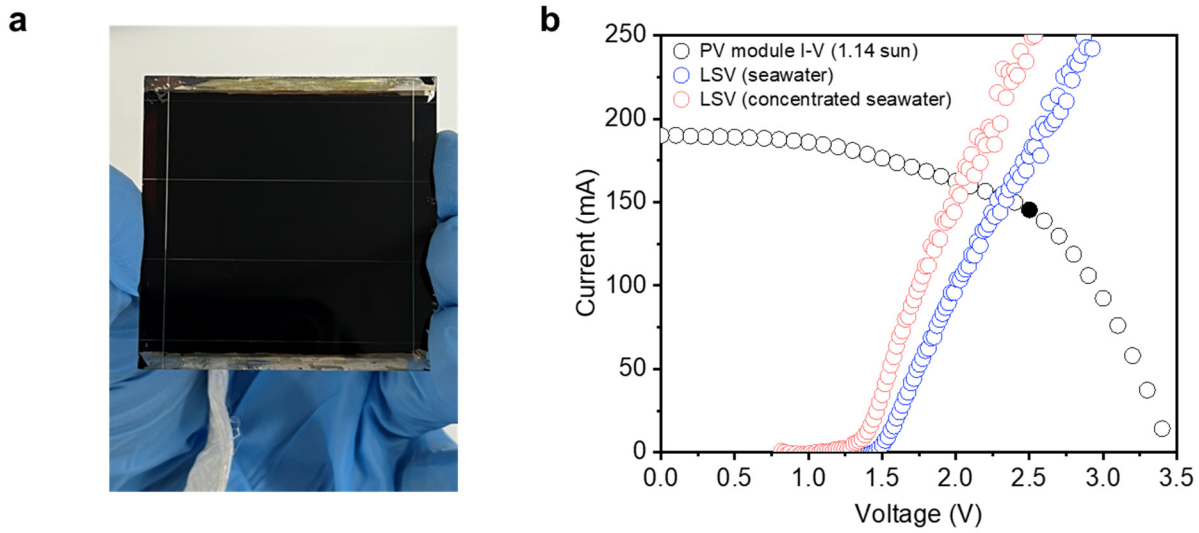

Fig. S89. (a) Picture of the perovskite-based PV module. (b) I-V cures of the perovskite-based PV module drawn together with LSV curves of the MEA system using seawater or concentrated seawater. The black dot represents the MPP of the PV module.